

Technical Progress Report

LOW TEMPERATURE CATHODE SUPPORTED ELECTROLYTES

DOE Contract No.: DE-AC26-99FT40710

For the period of

October 1, 1999 - March 31, 2000

Submitted by

Dr. Harlan U. Anderson
University of Missouri-Rolla
Electronic Materials Applied Research Center (EMARC)
303 Materials Research Center
Rolla, MO 65401

“This report was prepared as an account of work sponsored by an agency of the United States Government. Neither the United States Government nor any agency thereof, nor any of their employees, makes any warranty, express or implied, or assumes any legal liability or responsibility for the accuracy, completeness, or usefulness of any information, apparatus, product, or process disclosed, or represents that its use would not infringe privately owned rights. Reference herein to any specific commercial product, process, or service by trade name, trademark, manufacturer, or otherwise does not necessarily constitute or imply its endorsement, recommendation or favoring by the United States Government or any agency thereof. The views and opinions of authors expressed herein do not necessarily state or reflect those of the United States Government or any agency thereof.”

Executive Summary

October 1999 – March 2000

This project has three main goals: Thin Films Studies, Preparation of Graded Porous Substrates and Basic Electrical Characterization and Testing of Planar Single Cells.

During this time period substantial progress has been made in developing low temperature deposition techniques to produce dense, nanocrystalline yttrium-stabilized zirconia films on both dense oxide and polymer substrates. Progress has been made in the preparation and characterization of thin electrolytes and porous LSM substrates. Both of these tasks are essentially on or ahead of schedule.

In our proposal, we suggested that the ZrO_2/Sc system needed to be considered as a candidate as a thin electrolyte. This was because microcrystalline ZrO_2/Sc has a significantly higher ionic conductivity than YSZ, particularly at the lower temperatures. As a result, some 0.5 micron thick film of $ZrO_2/16\%$ Sc on an alumina substrate (grain size 20nm) was prepared and the electrical conductivity measured as a function of temperature and oxygen activity. The Sc doped ZrO_2 certainly has a higher conductivity than either 20nm or 2400nm YSZ, however, electronic conductivity dominates the conductivity for oxygen activities below 10^{-15} . Whereas for YSZ, electronic conductivity is not a problem until the oxygen activity decreases below 10^{-25} .

These initial results show that the ionic conductivity of 20nm YSZ and 20nm $ZrO_2/16\%$ Sc are essentially the same and the enhanced conductivity which is observed for Sc doping in microcrystalline specimens is not observed for the same composition when it is nanocrystalline. In addition they show that the electronic conductivity of Sc doped ZrO_2 is at least two orders of magnitude higher than that observed for YSZ.

The conclusion one reaches is that for 0.5 to 1 micron thick nanocrystalline films, Sc doping of ZrO_2 has no benefits compared to YSZ. As a result, electrolyte films of ZrO_2/Sc should not be considered as candidates. However, they have the potential of being useful as an interface on the anode side of the electrolyte.

NexTech has focused much of its effort during the past few months on establishing tape casting methods for porous LSM substrates. This work, performed under a separate DOE-funded program, involved tape casting formulations comprising LSM powders with bi-modal particle size distributions and fugitive pore forming additives. Sintered LSM substrates with porosities in the 30 to 40 vol% range, and pore sizes of 10~20 microns have been prepared. In addition, tape casting formulations involving composite mixtures of LSM and Sm-doped ceria (SDC) have been evaluated. The LSM/SDC cathode substrates are expected to provide better performance at low temperatures. Characterization of these materials is currently underway.

LOW TEMPERATURE CATHODE SUPPORTED ELECTROLYTES

TABLE OF CONTENTS

1.0: Abstract	4
2.0: Overview of Project.....	4
3.0: Individual Task Reports	5
Task 2.1: Thin Film Studies: Nanocrystalline Electrolyte	5
2.1.1: YSZ Thin Film Processing	5
2.1.2: ZrO₂/Sc Characterization	13
2.1.3: CeO₂ Characterization	14
Task 2.2: Preparation of Graded Porous Substrates	23
NexTech report	
Task 2.3: Basic Electrical Characterization and Testing of	
Planar Single Cells	27
2.3.1: Review of Impedance Spectroscopy	27
2.3.2: Specimen preparation for electrode and single	
cell characterization	36

1.0: Abstract

This project has three main goals or tasks:

Task 2.1: Thin Film Studies: Nanocrystalline Electrolyte

- 50% complete
- on schedule

Task 2.2: Preparation of Graded Porous Substrates

- 40% complete
- nearly on schedule

Task 2.3: Basic Electrical Characterization And Testing of Planar Single Cells

- 20% complete
- behind schedule, but most of the measurement obstacles have been overcome, so this task will come onto schedule in the 3rd quarter.

2.0: Overview of Project

In the first six months of this program:

1) Significant progress has been made in the preparation and characterization of thin electrolytes and porous LSM substrates. Both of these tasks (2.1 and 2.2) are essentially on or ahead of schedule. The results from these tasks are reported below in detail.

2) Task 2.3, Basic Electrical Characterization and Testing of Planar Single Cells is behind schedule primarily due to difficulties encountered in making reliable electrical contact to the single trilayer cells. As of May 2000, most of the problems have been solved and substantial progress is expected during the 3rd quarter of the project. Some of the preparation and measurement techniques are discussed below.

We are now able to produce dense 0.5 to 2 nm electrolyte films on the porous cathodes. The results on the YSZ/Sc system indicate that there is no advantage of using this system as the electrolyte (see details below). Therefore, the studies will be focussing on YSZ and CeO₂/Gd as the electrolyte. During the next six months, the program will spend most of its time on electrical measurements of trilayers as single cells and their microstructural characterization. By the end of this year, it is important that sufficient data have been taken to indicate which cathode and anode compositions need to be studied to optimize cell performance.

3.0: Individual Task Reports

Task 2.1: Thin Film Studies: Nanocrystalline Electrolyte

2.1.1: YSZ THIN FILM PROCESSING

(Brian Gorman)

THIN FILM YSZ ELECTROLYTE PROCESSING

Thin film electrolytes of $\text{ZrO}_2 : 16\% \text{Y}$ (YSZ) were produced on porous electrodes using a polymeric precursor spin-coating technique. Solutions consisting of distilled water and either ZrOCl_2 or $\text{Y}(\text{NO}_3)_3$ were standardized thermogravimetrically in order to find an exact concentration of cations in the solution. Accurately weighed amounts of these aqueous cation solutions were added in the appropriate stoichiometric concentrations along with ethylene glycol, tartaric acid and distilled water such that a 20 mol% cation solution was obtained. This solution was then heated and stirred at 70°C in order to drive off the excess water as well as the chloride and nitrate compounds. After approximately 72 hours, the solution was precipitate-free and had a viscosity of 80cps.

1 inch diameter single crystals of $\langle 100 \rangle$ NaCl (Marketech Intl., Inc.) were ground and polished using diamond impregnated polyethylene sheets (Allied High Tech Products, Inc.) to a surface roughness of $0.1\mu\text{m}$. After subsequent cleaning with 99% ethyl alcohol and drying in a dessicator, the YSZ polymeric precursor was spun on the NaCl substrates at 4000rpm for 30 seconds using a Brewer Science model CEE 100B spin coater. Immediately following the coating, the polymer film and NaCl substrate were transferred to a 70°C hotplate and cured for 2 hours in order to drive off the solvent and solidify the polymer film. Once the film had cured, the substrate and film were placed in a furnace on a ZrO_2 setter which were preheated to 350°C . After curing for approximately 3 minutes to pyrolyze the organics and form the oxide film, the substrates were transferred back to the 70°C hotplate and allowed to cool.

Presoaking the porous electrodes (to which the YSZ films will be transferred) in distilled water aids in the reduction of defects in the form of bubbles between the electrode and the transferred electrolyte. Placing the NaCl / YSZ structure in the water over the porous substrate with the YSZ film side down allows the YSZ film to float off of the NaCl and onto the porous substrate, which is then removed from the water and allowed to dry.

Initially, this experiment was conducted on porous cofired NiO / YSZ substrates. It was found at this point that when transferring a YSZ thin film to a porous substrate, a maximum film thickness of approximately $0.2\mu\text{m}$ can be transferred without cracking. Transferring thin films of 70nm to the porous NiO / YSZ substrate and annealing at temperatures ranging from 600 to 1000°C gives a crack-free YSZ film (figures 1 and 2). Ultimately, the processing temperatures used to produce these SOFC structures should be kept below approximately 600°C in order to take advantage of the nanocrystalline grain size effect on the ionic conductivity.

Subsequent transfers to the annealed YSZ surface and further annealing at 600°C can produce a thicker YSZ electrolyte. Spin coating of the YSZ precursor directly to the surface of

the YSZ film also increases the film thickness, depending upon the rotational speed of the spin chuck, the viscosity of the precursor and the cation concentration in the precursor. Unfortunately, it was also found that the reduction of NiO to Ni metal in the cermet caused localized cracking in the YSZ film (figure 3). Thus, it was decided to either pre-reduce the anode before transferring the YSZ film, which proved to be successful, or to transfer the YSZ film to the surface of a porous cathode. The latter method was the chosen focus.

CATHODE PROCESSING AND CATHODE-SUPPORTED THIN FILM SOFCS

Several advantages exist in using a cathode-supported electrolyte, as opposed to an anode-supported architecture. First, no reduction of oxides to metallic species would occur, minimizing the effects of the localized volume changes. Second, a high conductivity oxide with a thermal expansion similar to that of YSZ can be chosen to minimize stresses and overpotentials in the cell. Sr-doped Lanthanum Manganite (LSM) is a well-characterized material commonly used in conventional fuel cell cathodes, and it was chosen as the first candidate material for the cathode support. It has a thermal expansion coefficient similar to that of YSZ ($11.2 - 12.8 \times 10^{-6}$ cm/cm K depending upon the Sr doping concentration versus 10.8×10^{-6} for YSZ) and a high electronic conductivity (80 – 140 S/cm depending on the doping concentration and the temperature).

Powder of $\text{La}_{0.79}\text{Sr}_{0.20}\text{MnO}_3$ was fabricated using the Pechini method and calcined in an MgO crucible at 800°C for 4 hours. The powder was then milled with a water / polyethyleneglycol (PEG) mixture for 30 minutes and uniaxially pressed into 1.25cm diameter pellets at 15ksi. Sintering the pellets at 1100°C for 4 hours yielded a porous substrate to which the YSZ films could be transferred (figure 4). Transferring 70nm thick YSZ films to these pellets using the same technique as previously described for the anode-supported structure yielded severely cracked films. It was hypothesized that this cracking was due to surface roughness on the substrate and sharp corners of the LSM grains. To reduce these sharp corners on the surface of the LSM, the sintering temperature was increased to 1400°C, in an attempt to round off the grains on the surface (figure 5). After transferring and annealing 70nm thick YSZ electrolytes to these LSM pellets, it was found that there was a decrease in the amount of cracking that occurred, but a small amount of cracking did still occur.

$\text{La}_{0.84}\text{Sr}_{0.15}\text{MnO}_3$ powder was obtained from Praxair Specialty Ceramics. This powder was prepared using the glycine nitrate method, and then spray-annealed at 1400°C to yield spheroidized grains of LSM. As before, this powder was mixed and milled with water / PEG and uniaxially pressed at 15ksi in a 1.25cm diameter die. Sintering these substrates to 1450 and 1500°C yielded pellets with 23 and 17% porosity, respectively, as calculated from Archimedes data in kerosene. As can be seen from the SEM micrographs, figures 6 and 7, the surfaces of these substrates are more spherical than the LSM pellets fabricated by the Pechini method. Transferring YSZ films to these substrates lowered the amount of cracking significantly, but the increase in surface area of the LSM grains lowered the fraction of three-phase boundaries, which may ultimately lead to an increase in the cathode overpotential.

ANODE PRODUCTION

Silver was chosen as the anode for the LSM / thin film YSZ electrolyte configuration due to its high conductivity, catalytic activity, and increase in three-phase boundaries due to its decreased wetting of YSZ. 0.7 – 1.3 μm diameter powder was obtained from Alfa Aesar and three-roll milled with several different binder concentrations (Ferro Corporation). Surface SEM revealed that if the binder concentration is too low, a dense Ag layer is produced (figure 8). However, if too high of a binder concentration is used, the Ag is disconnected or does not cover enough surface area, as seen in figure 9. A reduction in three-phase boundary area leads to an increase in the anode overpotentials, and thus the power density. As can be seen in figure 9, 35 wt% binder with the Ag powder gives the greatest surface coverage, while not forming a dense layer. Figure 10 is an SEM cross section of a cell with an LSM cathode support, a 70 nm YSZ electrolyte (not visible in this micrograph due to the low magnification), and a porous Ag anode annealed at 600°C.

CELL PERFORMANCE TESTING

Figure 11 is a diagram of the cell testing apparatus used in this study. An LSM-supported YSZ electrolyte with a Ag anode annealed at 600°C can be mounted in the alumina support as shown using Pt paste on the air (cathode) side, and Ag paste on the forming gas (anode) side. After curing the seals at 600°C, the system should be gas-tight with the separation of hydrogen from air occurring only at the YSZ electrolyte surface. It was found recently that after extended periods of time at elevated temperatures, the Ag gas seal between the sample holder to the alumina support rod fails, presumably due to Ag migration along the surface of the alumina.

Presently, the connection method by which the anode is connected to the external voltage and current leads needs to be revised in order to obtain accurate data. Ohmic losses in the Pt leads which connect the sample to the external leads need to be accounted for, or larger gauge leads need to be used.

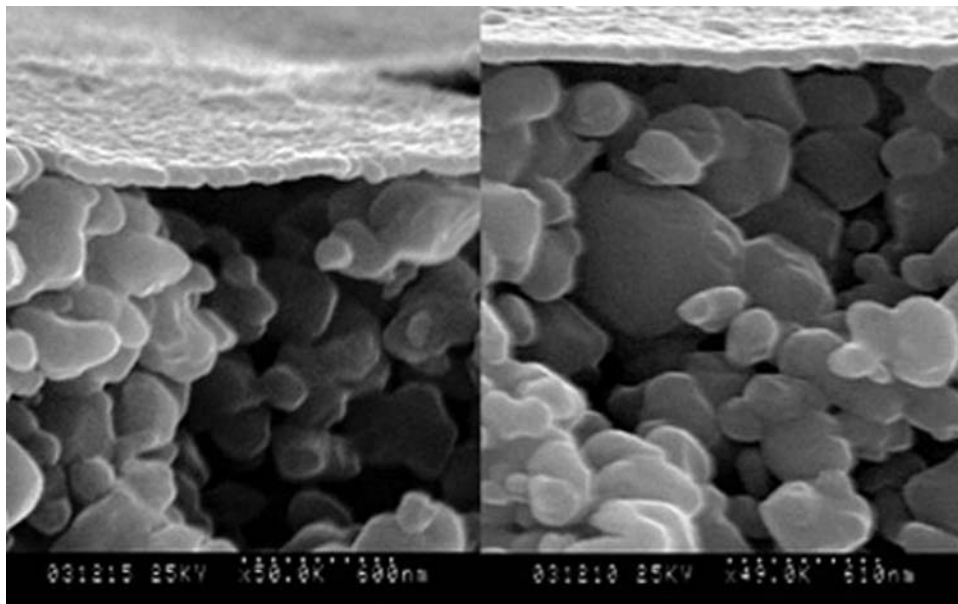


Figure 1. Cross sectional SEM micrograph of a 70nm thick YSZ electrolyte transferred to a porous NiO/YSZ composite and annealed at 1000°C

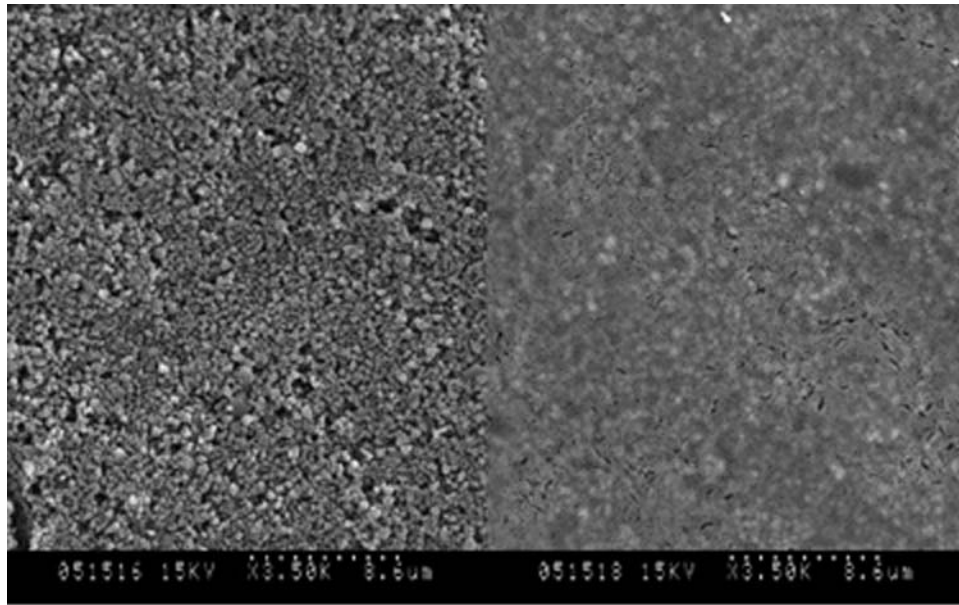


Figure 2. Surface SEM micrographs of NiO/YSZ before and after transferring a 70nm thick YSZ thin film and annealing at 1000°C

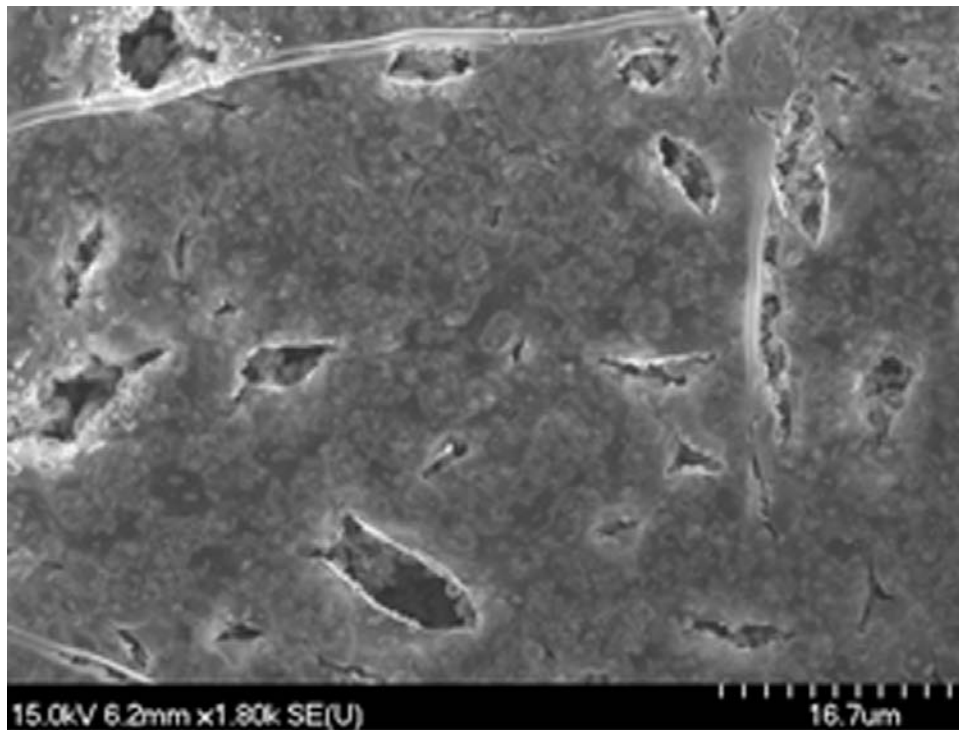


Figure 3. Surface SEM micrograph of a YSZ thin film showing localized cracking due to NiO reduction

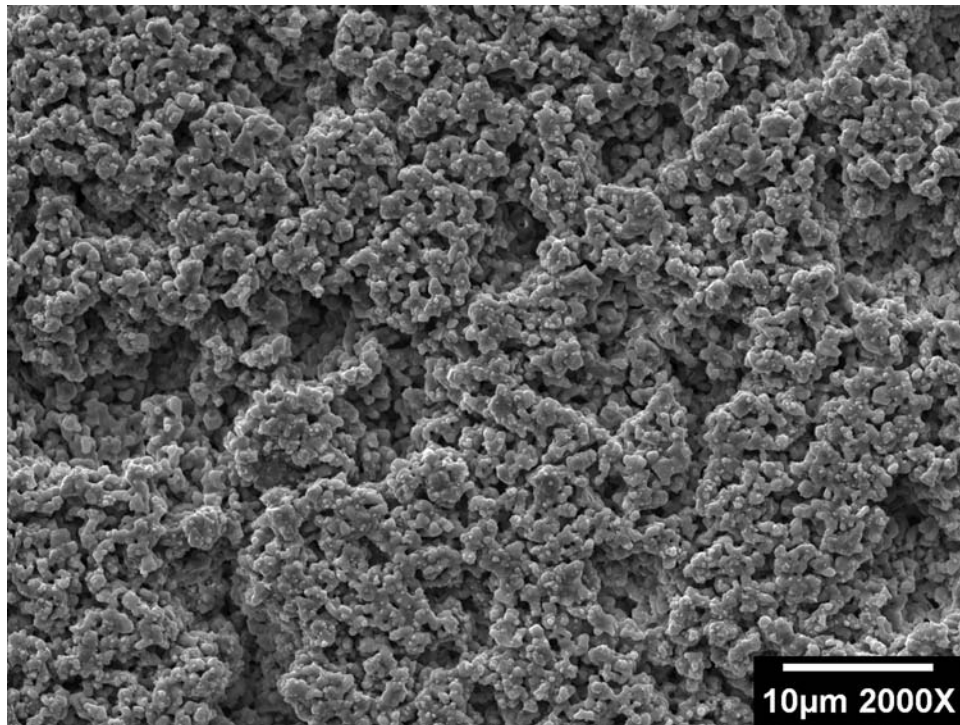


Figure 4. Surface SEM micrograph of a LSM pellet sintered at 1100°C for 4 hours

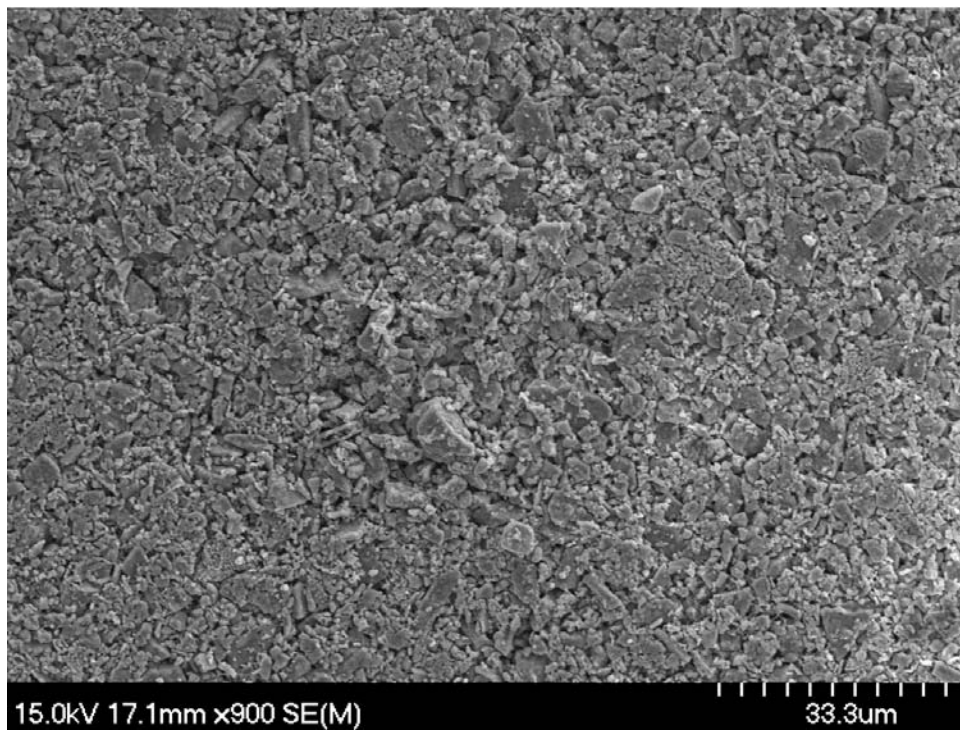


Figure 5. Surface SEM micrograph of a LSM pellet sintered at 1400°C for 4 hours

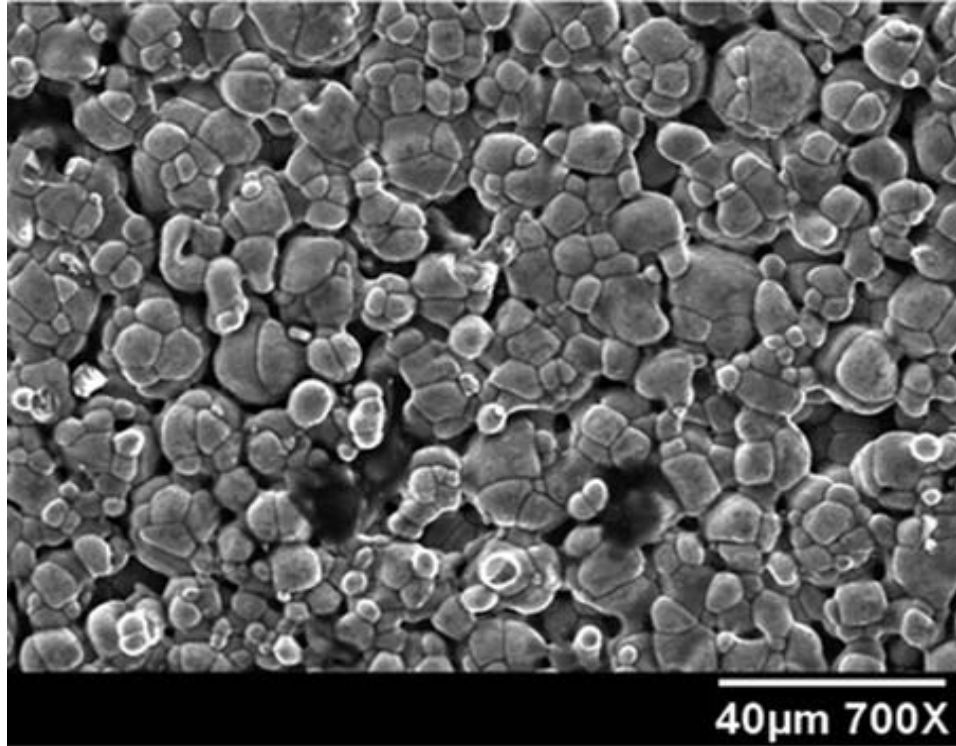


Figure 6. SEM micrograph of a Praxair LSM pellet surface sintered at 1450°C for 3 hours

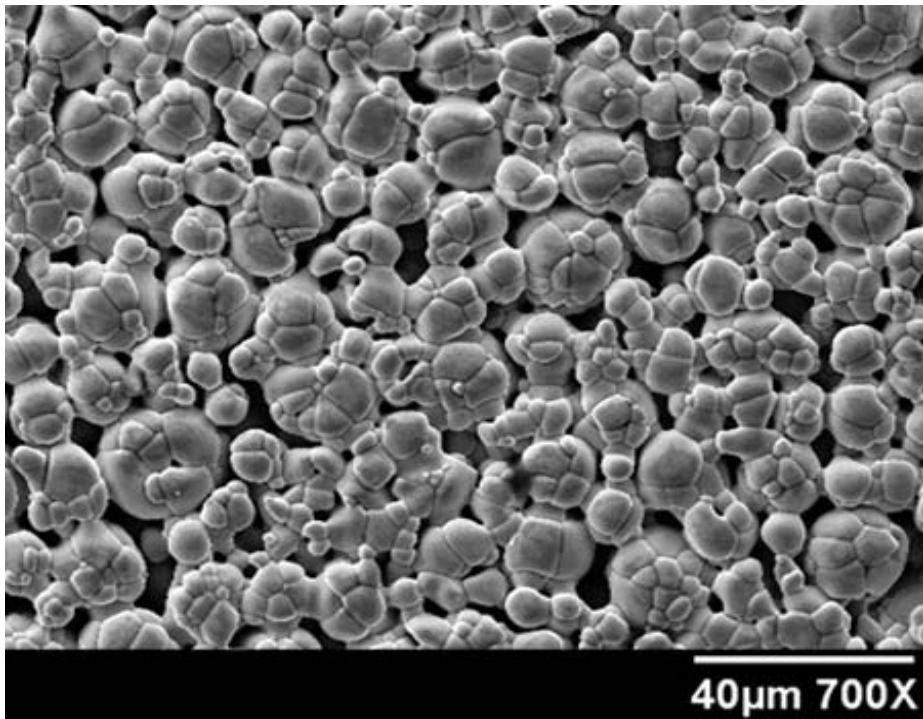


Figure 7. SEM micrograph of a Praxair LSM pellet surface sintered at 1500°C for 3 hours

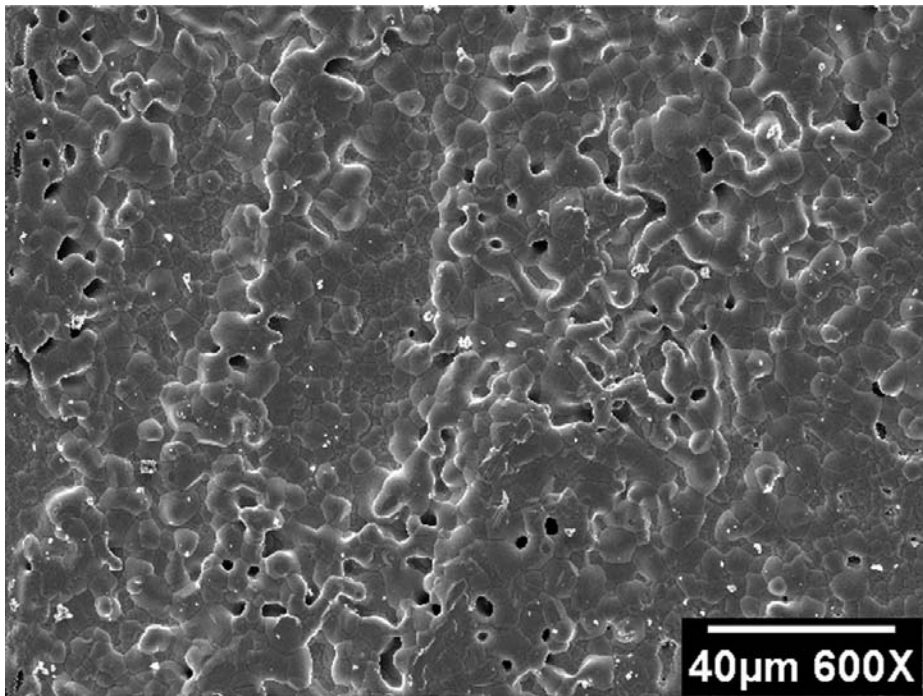


Figure 8. Surface SEM micrograph of a Ag anode annealed at 600°C with 15 wt% binder

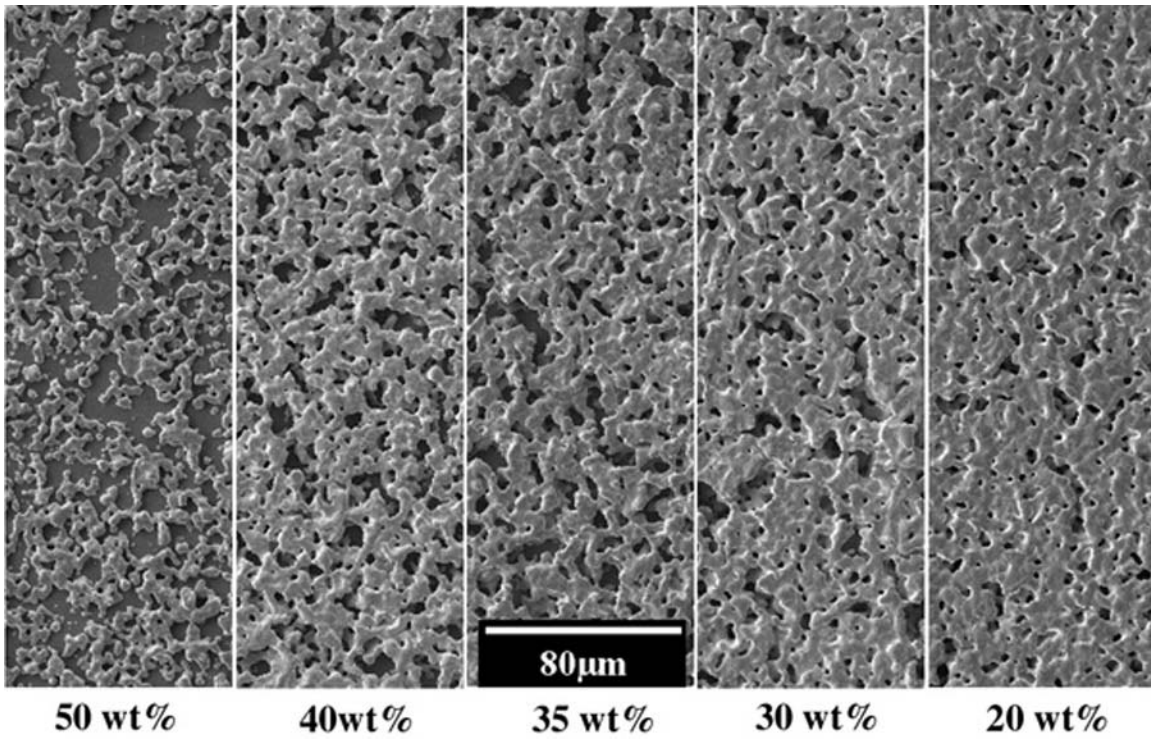


Figure 9. Ag surface coverage vs. wt% binder after annealing at 600°C for 2 hours

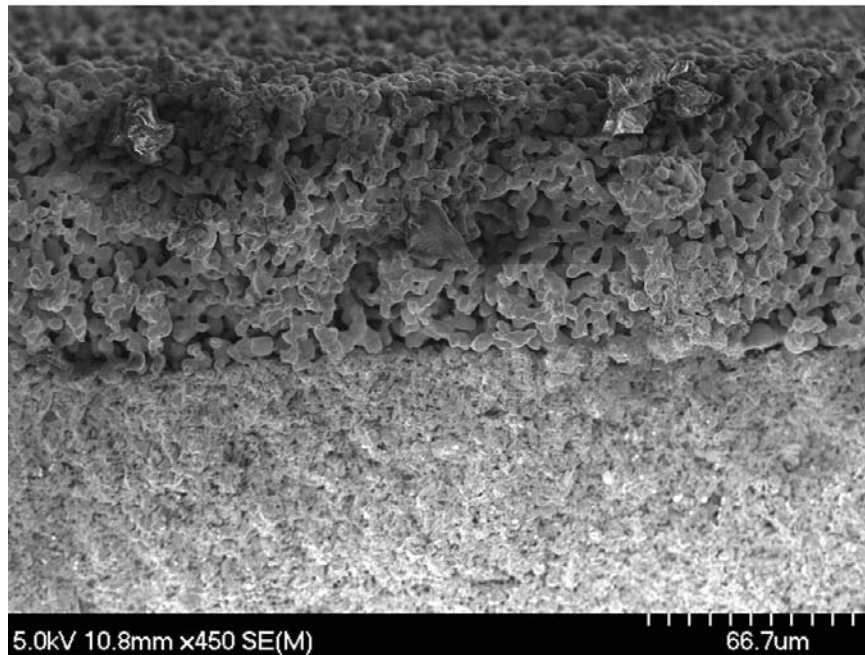


Figure 10. Cross-sectional SEM micrograph of a full thin film SOFC. The porous LSM substrate is visible on the bottom of the micrograph, with top surface the porous Ag anode.

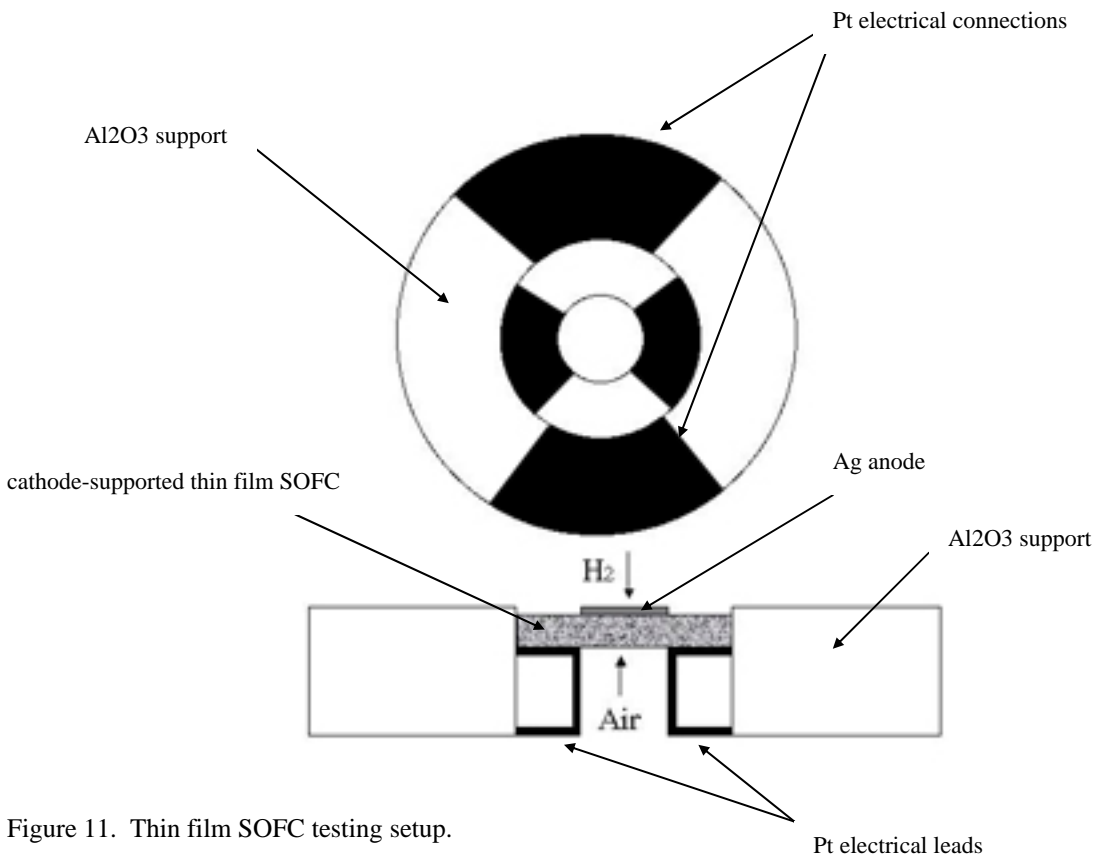


Figure 11. Thin film SOFC testing setup.

2.1.2: ZrO₂/Sc CHARACTERIZATION (Igor Kosacki)

In our proposal, we suggested that the ZrO₂/Sc system needed to be considered as a candidate as a thin electrolyte. This was because microcrystalline ZrO₂/Sc has a significantly higher ionic conductivity than YSZ, particularly at the lower temperatures. As a result, some 0.5 micron thick film of ZrO₂/16% Sc on an alumina substrate (grain size 20nm) was prepared and the electrical conductivity measured as a function of temperature and oxygen activity. As can be seen in figure 1, at 900°C, the Sc doped ZrO₂ certainly has a higher conductivity than either 20nm or 2400 nm YSZ, however, electronic conductivity dominates the conductivity for oxygen activities below 10⁻¹⁵(exp). Whereas for YSZ, electronic conductivity is not a problem until the oxygen activity decreases below 10⁻²⁵(exp). Figure 2 shows the temperature and oxygen activity dependence of the electrical conductivity and figures 3 and 4 show the temperature dependence of the electronic and ionic conductivity at one atm. oxygen.

These initial results show that the ionic conductivity of 20 nm YSZ and 20nm ZrO₂/16%Sc are essentially the same and the enhanced conductivity which is observed for Sc doping in microcrystalline specimens is not observed for the same composition when it is nanocrystalline. In addition they show that the electronic conductivity of Sc doped ZrO₂ is at least two orders of magnitude higher than that observed for YSZ.

The conclusion one reaches is that for 0.5 to 1 micron thick nanocrystalline films, Sc doping of ZrO₂ has no benefits compared to YSZ. As a result, electrolyte films of ZrO₂/Sc will not be considered as candidates for this program. Since, the specimens have already been prepared, the characterization studies will be completed and the results published.

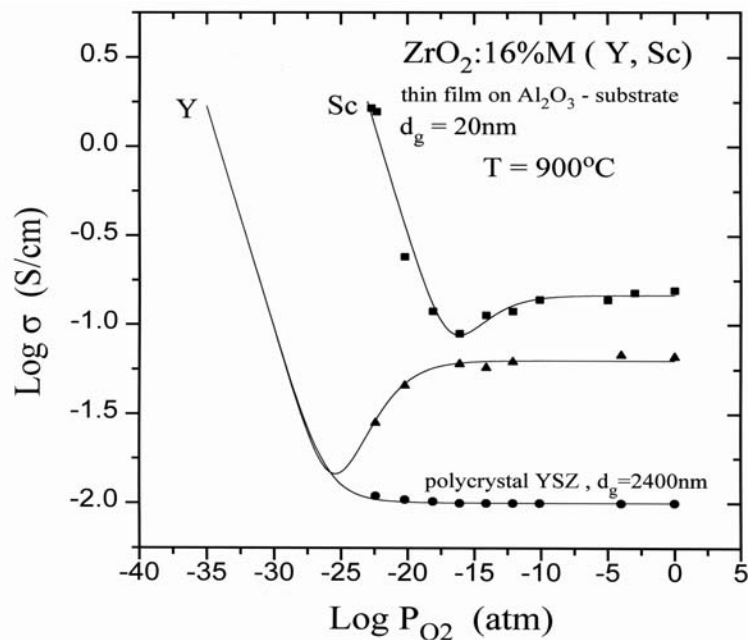


Figure 1

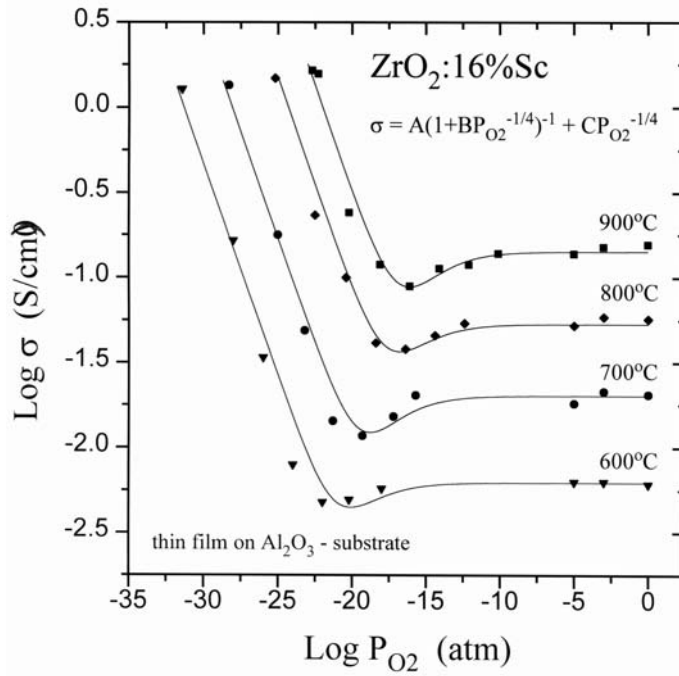


Figure 2

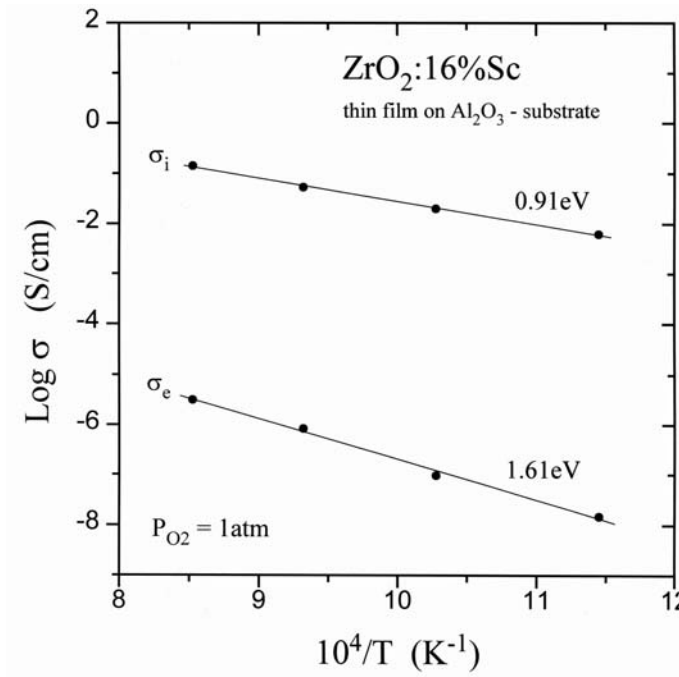


Figure 3

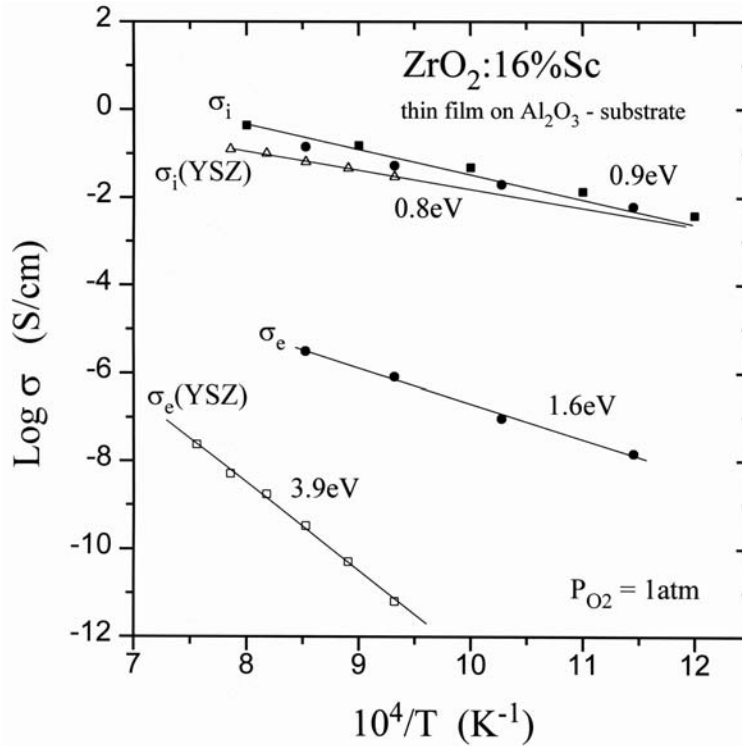


Figure 4

2.1.3: CeO₂ CHARACTERIZATION
(Toshio Suzuki and Igor Kosacki)

Presented at the 102nd Annual Meeting and Exposition
of the American Ceramic Society, May 1, 2000

**ELECTRICAL TRANSPORT AND DEFECT THERMODYNAMICS IN
NANOCRYSTALLINE CeO₂**

Toshio Suzuki, Igor Kosacki and Harlan U. Anderson
Electronic Materials Applied Research Center,
University of Missouri-Rolla, Rolla, MO 65401

ABSTRACT

The results of a study of the electrical properties of CeO₂ thin films obtained by a polymeric precursor spin coating technique are presented. The electrical conductivity has been studied as a function of temperature and oxygen activity and correlated with the grain size. When compared to microcrystalline specimens, nanocrystalline specimens showed enhanced electronic conductivity and different stoichiometry which are related to microstructure. The transition from extrinsic to intrinsic type of the conductivity has been observed as the grain size decreases below

100nm and it is shown that the enthalpy of formation for oxygen vacancies in CeO₂ becomes greatly reduced.

INTRODUCTION

Nanocrystalline materials are of interest due to their ability to improve the electrical transport and catalytic activity. Understanding this mechanism is of importance for the development of electroceramic devices, such as gas sensors, fuel cells and ionic membranes [1, 2, 3, 4]. For such devices, CeO₂ has been one of candidates and intensively studied. Microcrystalline CeO₂ is characterized as an extrinsic conductor, whose conductivity is related to impurity effect, while nanocrystalline CeO₂ shows an intrinsic conductivity. It is also shown that there is an increase of over 4 orders of magnitude in the electronic conductivity of nanocrystalline CeO₂ (10nm grain size) compared with microcrystalline CeO₂ (5 micron grain size) [5, 6]. However, few experimental data are available related to the influence of microstructure on properties, because of difficulties in stabilizing the microstructures. To meet this requirement, the polymeric precursor spin coating technique has proven to be useful since it allows the formation of dense nanocrystalline thin film materials at lower temperatures. This method has recently used for preparation of nanocrystalline oxides of ZrO₂:Y[7], CeO₂[8] and SrCeO:Yb[3].

The purpose of this study is to understand how microstructure influences the electrical transport and thermodynamic parameters of CeO₂ thin films. The electrical measurements of CeO₂ with different microstructure as a function of temperature and oxygen activity have been performed systematically over the grain size range from 10 to 270nm.

MICROSTRUCTURE OF NANOCRYSTALLINE CeO₂

The polymer precursor technique was used to prepare nanocrystalline dense CeO₂ specimens[9]. The films were prepared by spin coating a polymer precursor solution onto a substrate. The solutions were prepared by quantitatively dissolving water soluble cation sources such as nitrates and carbonates into solutions which contain chelating and polymerizing agents such as ethylene glycol and water. Figure 1 shows SEM images of the surface and the cross-section of a CeO₂ thin film deposited on a monocrystalline sapphire substrate, annealed at 600, 800, 1000°C for 4hrs. As can be seen in Fig.1(b), this film is dense with the thickness of about 0.3µm. Its thickness is dependent upon the number of depositions and the concentration of the precursor. For this case, 13 depositions of a 2wt% precursor were applied. Since the nucleation of the oxides from the polymeric precursor occurs on the molecular level, the films are characterized by very uniform microstructures. As seen in Fig.1, the films possess a uniform grain size distribution and a dense microstructure.

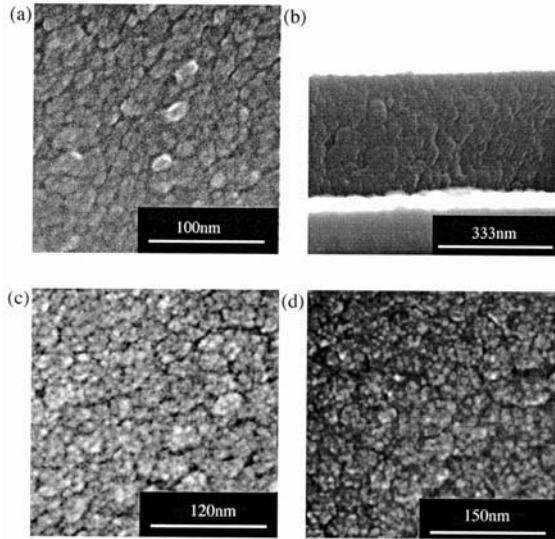


Figure 1. SEM images of CeO₂ thin film deposited on a sapphire substrate. Films are annealed 4hrs at (a) 600°C (surface:10nm) (b) 600°C (cross-section) (c) 800°C (surface:20nm) (d) 1000°C (surface:65nm)

Figure 2 shows the XRD patterns obtained for CeO₂ specimens annealed at different temperatures along with the standard patterns for CeO₂ and Al₂O₃. All samples were annealed for 4hrs. Note that for temperature below 1000°C no preferential orientation is observed. However at 1000°C an out-of-plane texture growth is observed. For temperatures higher than 1000°C in-plane texturing starts to occur with preferential orientation of (200). The inserted figure in Fig.2 shows the grain size of films deposited both sapphire and polycrystalline Al₂O₃ substrates as function of annealing temperature. The grain size is determined by the analysis of the shape of X-ray lines shown in Fig.2. As can be seen, grain size has little dependence on the substrates, but varies from 4 to 450nm over the annealing temperature range of 400-1200°C.

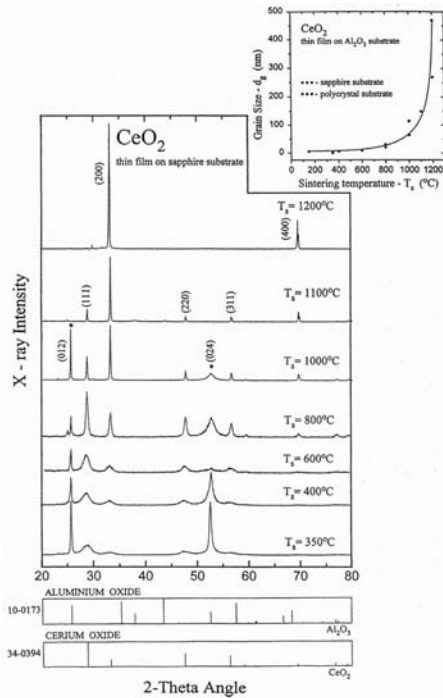


Figure 2. X-ray diffraction patterns of CeO₂ thin films (inserted Figure: The dependence of grain size with sintering temperature)

DEFECT MODEL AND ELECTRICAL CONDUCTIVITY

From the measurements of electrical conductivity as a function of oxygen partial pressure and temperature, it is possible to obtain the information about the type of conductivity and thermodynamic parameters of the defects. The results of this study are interpreted by the model as shown below. Based on the assumption that only ionic and electronic conductivity (σ_i and σ_e) exist and that they are controlled by the oxygen vacancy and electron concentration, respectively, and that the electron transport is attributed to small polaron hopping with a thermally activated electron mobility, then the expression for total conductivity is given by

$$\sigma = \sigma_i + \sigma_e \quad (1)$$

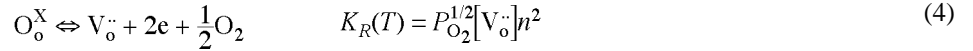
where

$$\sigma_i = 2e[V_{\text{o}}^{\cdot\cdot}] \mu_{V_{\text{o}}^{\cdot\cdot}} \quad (2)$$

and

$$\sigma_e = ne\mu_e = ne\left(\frac{\mu_0}{T}\right) \exp\left(-\frac{E_h}{kT}\right) \quad (3)$$

e , μ_0 , E_h , n and $[V_{\text{o}}^{\cdot\cdot}]$ are the charge of an electron, a temperature independent constant in the expression for mobility, the hopping energy, the electron and oxygen vacancy concentration, respectively. In this region, ionic defects can be introduced by the reaction as follows,



More generally, ignoring defects on the cation sublattices, the electroneutrality relation is given by

$$2[V_{\text{o}}^{\cdot\cdot}] = [A'] + n \quad (5)$$

in which A' is acceptor impurity.

The stoichiometry is determined by Eq. 4 and the temperature dependence of the equilibrium constant is given by

$$K_R(T) = K_R^0 \exp\left(-\frac{\Delta H}{kT}\right) \quad (6)$$

where ΔH is the enthalpy for oxygen vacancy formation.

Combining Eqs. 3, 4 and 6, the electronic conductivity as a function of temperature is given by

$$\sigma_e T = \sigma_0 \exp\left(-\frac{E_{act}}{kT}\right) P_{\text{O}_2}^{-r} \quad (7)$$

where σ_0 is electronic conductivity which is temperature independent, E_{act} is the activation energy and r is the power factor of P_{O_2} , which is determined by the mechanism of charge compensation.

For the extrinsic region ($[A'_{Ce}] = 2[V_{\delta}]$), the conductivity and oxygen partial pressure exhibit the power relationship with the slope of $r = 1/4$. The activation energy calculated for this region from the relation of $\ln(\sigma_e T)$ as a function of T^{-1} is

$$E_{act} = \frac{\Delta H}{2} + E_h \quad (8)$$

In the intrinsic region ($n = 2[V_{\delta}]$), the $\log \sigma$ vs $\log P_{O_2}$ relationship should follow the slope of $r = 1/6$ and temperature dependence of the conductivity gives an activation energy equal to

$$E_{act} = \frac{\Delta H}{3} + E_h \quad (9)$$

The concentration of oxygen vacancy from intrinsic reaction (Eq. 4) can be described as

$$[V_{\delta}]_i = N_0 \exp\left(-\frac{S_{V_{\delta}}}{2k}\right) \exp\left(-\frac{\Delta H}{2kT}\right) \quad (10)$$

where N_0 is the number of sites per unit volume [10]. $S_{V_{\delta}}$ is the entropy of oxygen vacancy given as

$$S_{V_{\delta}} = S(vib) - k \ln X_{V_{\delta}} \quad (11)$$

where $X_{V_{\delta}}$ is the site fraction of the oxygen vacancy, $X_{V_{\delta}} = [V_{\delta}]_i / N_0$. $S(vib.)$ is the vibrational term, which is small compared with the second term and can be negligible [11]. Using Eq10 and 11, $[V_{\delta}]_i$ can be calculated in terms of ΔH and temperature,

$$[V_{\delta}]_i = N_0 \exp\left(-\frac{\Delta H}{3kT}\right) \quad (12)$$

ELECTRICAL CONDUCTIVITY OF NANOCRYSTALLINE CeO₂

The electrical conductivity of 0.3 micron thick films has been studied by impedance spectroscopy. The impedance spectra are being obtained using a 2-probe measurement over the frequency range 1 Hz to 5 MHz. Silver is being applied as electrodes for these measurements. Measurements are being conducted in oxygen, air, helium and CO/CO₂ mixtures for the oxygen partial pressure range of 10^{-26} - 1atm over the temperature range of 600-900°C.

Figure 3 shows the electrical conductivity of films whose grain size varies from 20nm to 150nm as a function of P_{O_2} and temperature. As can be seen in Fig.3(a), the electrical conductivity of the 150nm grain size sample is independent with P_{O_2} at high P_{O_2} , follows $P_{O_2}^{-1/4}$ behavior at low P_{O_2} , which is seen also for microcrystalline specimens[8]. This behavior is considered to be related to impurity effect. On the other hand, the electrical conductivity of the 65 and 30nm specimens displayed in Fig.3(b) and (c) show the transition from $P_{O_2}^{-1/4}$ to $P_{O_2}^{-1/6}$ behavior with increasing temperature. The $P_{O_2}^{-1/6}$ relationship corresponds to the intrinsic charge compensation, $n = 2[V_{\delta}]$. It is seen that the onset temperature for intrinsic behavior decreases as grain size decreases until only intrinsic is observed for 20nm grain size (Fig.3(d)). However, for $d_g = 20$ nm at lower P_{O_2} the P_{O_2} dependence decreases below $-1/6$. This suggests a change in either the model or compensation mechanism. It is possible that at the lower grain size, that surface and

grain boundary effects dominate the exchange reactions because of the increased grain boundary volume and surface area. This supposition is supported by the study of Horita, et al who measured oxygen surface exchange for $Y_{0.2}Ce_{0.8}O_{2-x}$ and showed that the surface exchange coefficient varied with $P_{O_2}^{-1/20}$ [12]. This may explain the behavior seen in Fig.3(d), but further investigation is required.

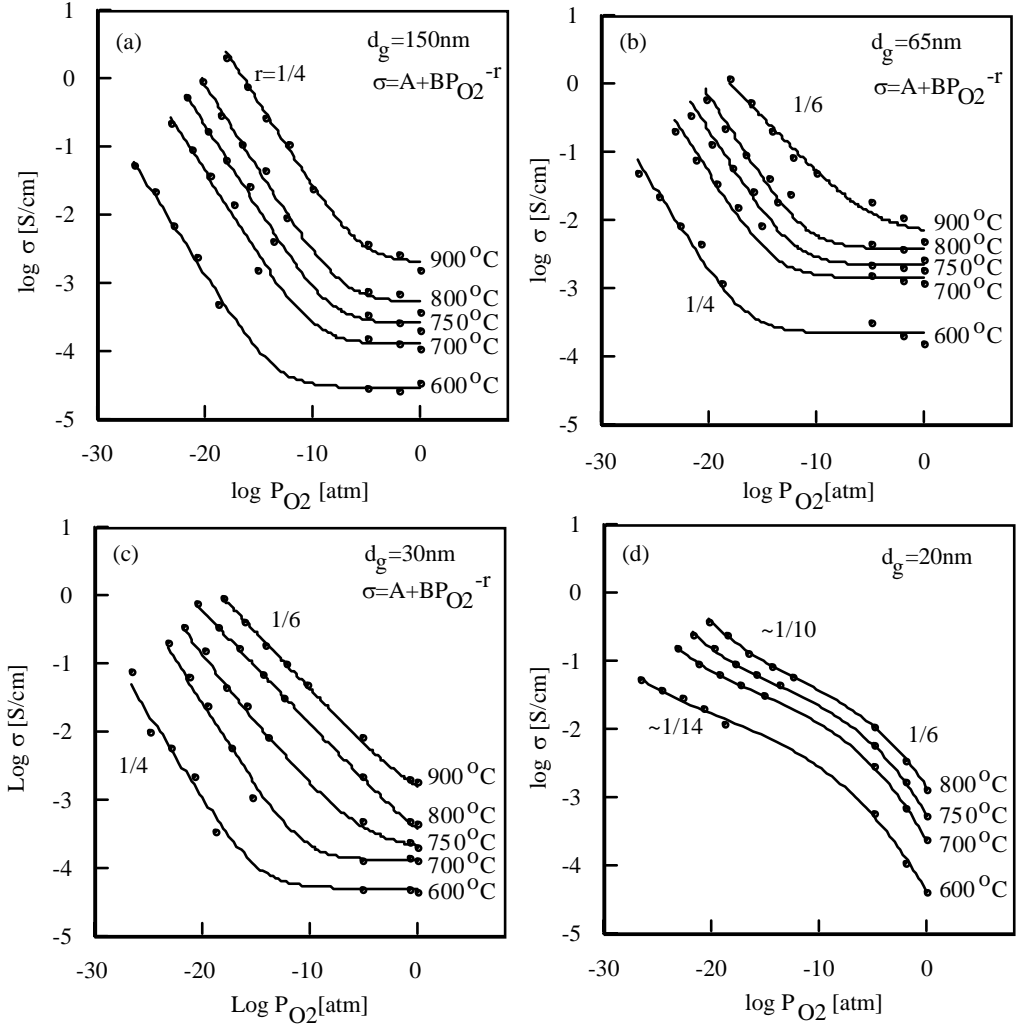


Figure 3. The electrical conductivity of CeO_2 thin film as a function of P with different temperature. (a) grain size 150nm (b) grain size 65nm (c) grain size 30nm (d) grain size 20nm.

Equation 1 is used to deconvolute and determine the electronic conductivity. Figure 4 shows the temperature dependence of the electronic conductivity determined for different grain size specimens at $P_{O_2}=1\text{atm}$. It is observed that the electronic conductivity increases and activation energy decreases as the grain size d_g decreases. The discontinuity observed for the 30nm grain size sample is related to the transition seen in Fig.3(c).

The enthalpy of oxygen vacancy formation ΔH was also calculated using the relation shown in Eq. 8 and 9, assuming an electron hopping energy of $E_h=0.4\text{eV}$ [13] Figure 5(a) shows ΔH as a function of grain size. It is seen that ΔH decreases for grain size less than 100nm, which

implies greater deviation from stoichiometry, which in turn increases the electrical conductivity. The values of ΔH determined for greater than 100nm grain size specimens agree with the value reported for single crystal CeO_2 , which was reported as $\Delta H=4.67\text{eV}$ [5].

Using the value of ΔH , the defect concentration can be calculated by Eq.12, assuming that the defect is created based on the nonstoichiometry given by the reaction shown in Eq.4 during annealing. These results are shown in Fig.5(b). It is seen that there is good correlation between the estimations obtained from electrical measurements and previous data from coulometric titration and transport measurements[6,14,15].

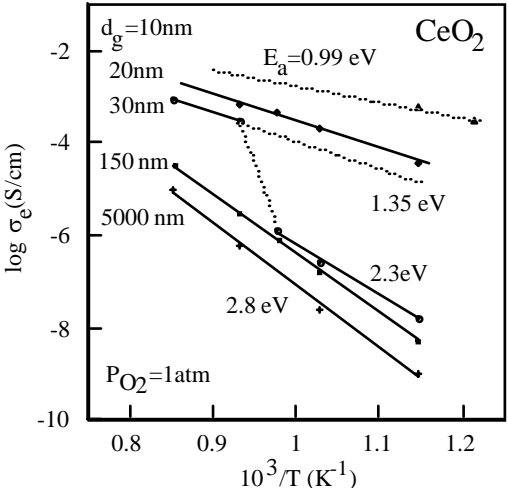


Figure 4. Temperature dependence of electronic conductivity determined for CeO_2 with different microstructure

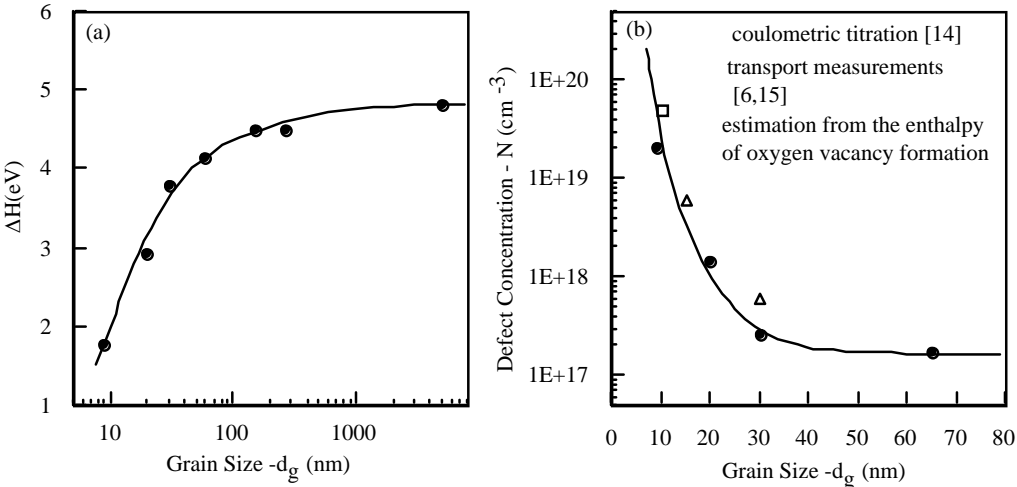


Figure 5. (a) The enthalpy of oxygen vacancy formation of CeO_2 thin film and (b) the defect concentration as a function of microstructure.

CONCLUSIONS

The results of a study related to the formation and the microstructure of CeO_2 thin films obtained by a polymeric precursor spin coating technique have been presented. Using this preparation method, it was possible to obtain dense thin films (0.3 micron thick) with grain size

in the nanometer range (4-300nm) on the sapphire substrates. The electrical properties of these films have been investigated as a function of grain size, temperature and oxygen partial pressure. The results show that the electrical conductivity of nanocrystalline CeO₂ increases as the grain size decreases. From the results of electrical measurement, it was possible to determine the enthalpy of oxygen vacancy formation, ΔH , as a function of grain size. This reduction of ΔH at grain size lower than 100nm leads to an increase of nonstoichiometry. This is a unique and remarkable result since it shows that microstructure can change the stoichiometry. The defect concentration is also estimated from the value of ΔH as a function of grain size. This result shows good correlation with the data from coulometric titration and transport measurements.

ACKNOWLEDGEMENT

The authors wish to thank the Department of Energy, Contract #DE-AC26-99FT40710 for partial support of this research.

REFERENCES

- [1] G. M. Christie and F.P.F. van Berkel, Microstructure - ionic conductivity relationships in ceria-gadolinia electrolytes, *Solid State Ionics* 83 pp. 17-27, 1996.
- [2] M. Mogensen, T. Lindegaard, U. R. Hansen and G. Mogensen, Optimizing mixed conductor SOFC anodes of doped CeO₂, *Ionic and mixed conducting ceramics 2nd international symposium* pp. 448-465, 1994.
- [3] I. Kosacki and H. U. Anderson, The structure and electrical properties of SrCe_{0.95}Yb_{0.05}O₃ thin film protonic conductors, *Solid State Ionics* 97 pp. 429-436, 1997.
- [4] I. Kosacki and H. U. Anderson, Nanostructured oxide thin films for gas sensors, *Sensors and Actuators B* 48 pp. 263-269, 1998.
- [5] Y. -M. Chiang, E. B. Lavik, I. Kosacki, H. L. Tuller, and J. Y. Ying, Defect and transport properties of nanocrystalline CeO_{2-x}, *Appl. Phys. Lett.* 69 2 pp. 185, 1996.
- [6] I. Kosacki and H. U. Anderson, Electrical conductivity and structure of nanocrystalline CeO₂ thin films, *Mat. Res. Soc. Symp. Proc. Vol. 453* pp.537, 1997.
- [7] I. Kosacki, B. Gorman and H. U. Anderson, Microstructure and electrical conductivity in nanocrystalline oxide thin films, *Electrochemical Society Proceedings*, 97(24),631, 1998.
- [8] I. Kosacki, T. Suzuki, and H. U. Anderson, Nanocrystalline oxide thin films for electrochemical devices, *Proceeding of 195th meeting of Electrochem. Soc.*, 99-13,190—198, 1999.
- [9] H. U. Anderson, M. M. Nasrallah, C. C. Chen, Method of coating a substrate with a metal oxide film from an aqueous solution comprising a metal cation and a polymerizable organic solvent, U.S. Patent 5494700, 1996
- [10] G. A. Samara, Pressure and temperature dependences of the ionic conductivities of cubic and orthorhombic lead fluoride PbF₂, *J. Phys. Chem. Solids* 40 pp.509-522, 1978.
- [11] R. J. Panlener, R. N. Blumenthal and J. E. Garnier, A thermodynamic study on nonstoichiometric cerium dioxide, *J. Phys. Chem. Solids*, Vol. 36 pp.1213-1222, 1975.
- [12] T. Horita, K. Yamaji, N. Sakai, M. Ishikawa, H. Yokokawa, T. Kawada, and M. Dokiya, Oxygen surface exchange of Y_{0.2}Ce_{0.8}O_{2-x} under reducing atmosphere, *Electrochem. and solid-state lett.*, 1(1) . pp.4-6, 1998.
- [13] H. L. Tuller and A. S. Norwick, Small polaron electron transport in reduced CeO₂ single crystals, *J. Phys. Chem. Solids*, Vol. 38 pp.859-867, 1977.

[14] O. Porat and H. L. Tuller, Simplified analytical treatment of defect equilibria: Applications to oxides with multivalent dopants, *J. Electroceramics* 1:1, pp. 41-49, 1997.

[15] J. Hwang and T. O. Mason, Defect chemistry and transport properties of nanocrystalline cerium oxide, *Zeit. Phys. Chem. Bd. 207*, pp. 21-38, 1998.

Task 2.2: Preparation of Graded Porous Substrates

(NexTech Report)

OVERVIEW/GOALS

In the first six months of this project, NexTech Materials has taken several steps to design bilayer substrates of $\text{La}_x\text{Sr}_{(1-x)}\text{MnO}_{3-\delta}$ (LSM) and $\text{Ce}_x\text{Sm}_{(1-x)}\text{O}_{2-\delta}$ (SDC) with the appropriate size, morphology and composition for UMR’s polymeric thin-film deposition route. The bilayer strategy selected for this program is shown schematically in Figure 1. A 1-1.5 mm thick substrate layer provides the structural support and gas transport path for the fuel gases to the interfacial and electrolyte layers. A much thinner (~2-10 μm) composite interfacial layer consisting of LSM mixed with SDC smoothes the deposition surface and prevents wicking of the polymer precursor into the substrate by presenting a surface with porosity ~0.5 μm diameter. The addition of SDC to LSM has been shown to improve electrode performance at moderate temperatures, and reduces the YSZ/LSM interfacial area, which should limit LSM/YSZ interaction at the required processing temperatures. The development of the bilayer is being carried out by simultaneously pursuing tape casting and lamination methods for producing the substrate layer, while developing methods to deposit the LSM/SDC composite interface layer.

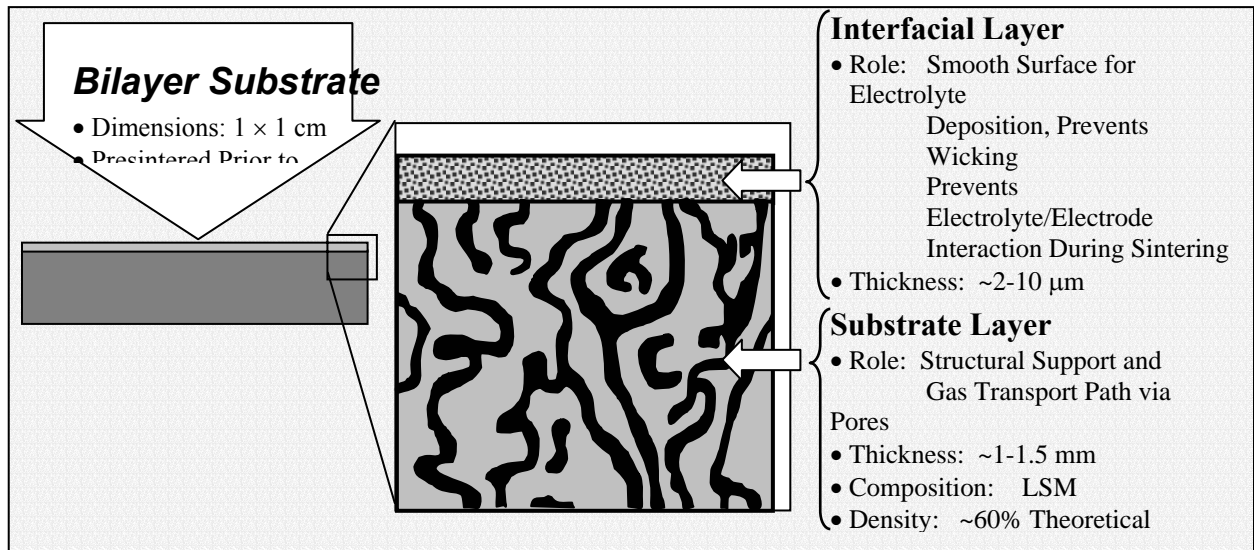


Figure 1. Bilayer Substrate Schematic and Target Properties

SUBSTRATE DEVELOPMENT

NexTech has focused much of its effort during the past few months on establishing tape casting methods for porous LSM substrates. This work, performed under a separate DOE-funded program, involved tape casting formulations comprising LSM powders with bi-modal particle size distributions and fugitive pore forming additives. Sintered LSM substrates with porosities in the 30 to 40 vol% range, and pore sizes of 10~20 microns have been prepared. In addition, tape casting formulations involving composite mixtures of LSM and Sm-doped ceria (SDC) have been

evaluated. The LSM/SDC cathode substrates are expected to provide better performance at low temperatures. Characterization of these materials is currently underway.

Initial investigations of LSM substrate densification resulted in many microstructures similar to that shown in Figure 2. The large-scale porosity has a diameter close to the desired dimension, but fine scale pores within the solid 'webs' are problematic. The small pores increase the porosity of the sample, but serve as dead zones for gas transport to and from the electrolyte.

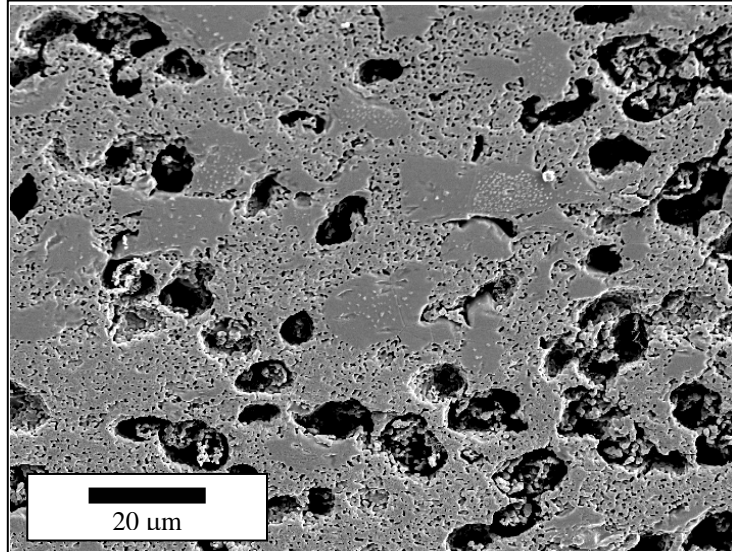


Figure 2. Micrograph of LSM Substrate Layer with Bimodal Porosity.

To overcome the insufficient densification of the solid web, a set of experiments was designed to evaluate new sintering strategies. To enhance the sintering performance, LSM powder that had been ground to $\sim 1\mu\text{m}$ average particle size was used in the experiments. In addition, V_2O_5 and a $\text{CuO}/\text{Cu}_2\text{O}$ mixture were used to lower the sintering temperature and increase densification. To evaluate the effect of fugitive additions, additions of 50 and 25 wt% maltodextrin were made to pellets of the same compositions. Pellets were fired under conditions between 1100°C , 3h and 1400°C , 1h, and the densities were evaluated by Archimedes' method.

Figure 3 shows the effect of 0.5 wt% V_2O_5 and $\text{CuO}/\text{Cu}_2\text{O}$ on the densification of LSM. The copper oxide eutectic composition has little effect on densification, showing only a minor deviation at temperatures $\sim 1250^\circ\text{C}$, where a slight increase in density is observed. However, the V_2O_5 addition has a strong effect on density at all temperatures above 1100°C , increasing the measured density by $\sim 10\%$ in the temperature range $1200\text{-}1400^\circ\text{C}$. It is expected that this effect may increase with further V_2O_5 additions. In future experiments, amounts up to 2 wt% V_2O_5 will be added to the LSM, and its effect on densification evaluated. It is expected that at these low levels of V_2O_5 , there will be little detrimental effect on the electrical properties of the material. However, testing of this theory is merited. If these effects are confirmed to be negligible, the V_2O_5 addition is an attractive route for increasing LSM densification at low temperature.

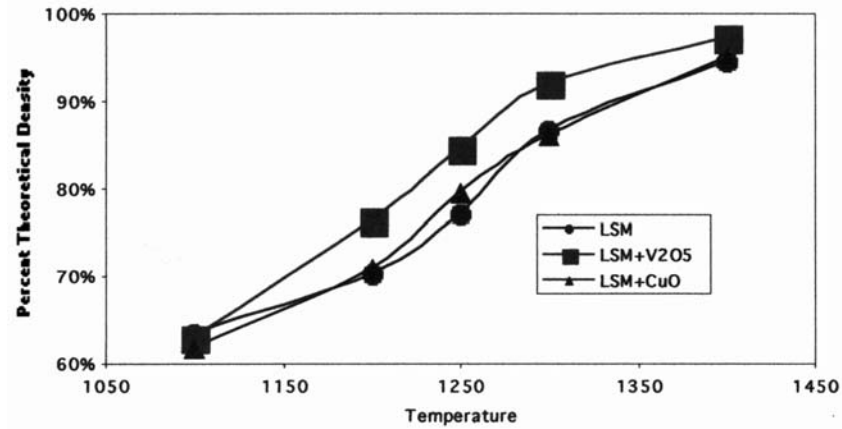
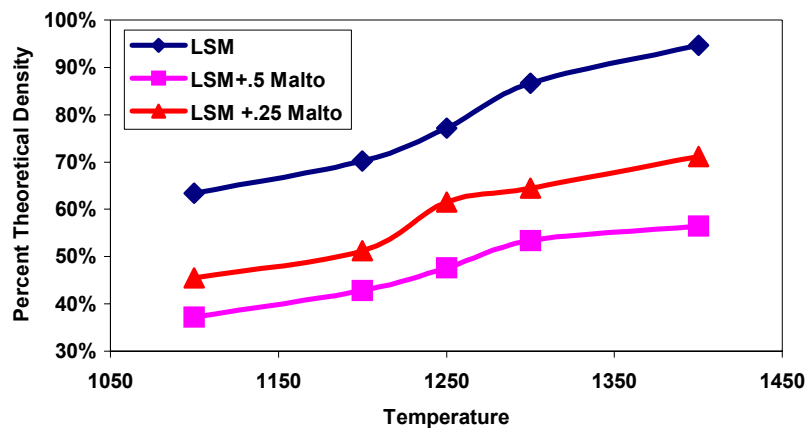
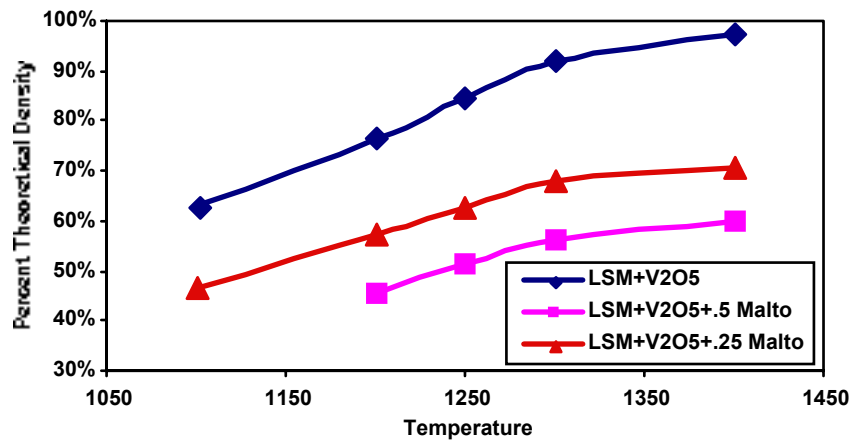


Figure 3. Densification v. Temperature, Effect of Liquid Phase Formers

To investigate the effect of fugitive additions on LSM densification with and without liquid phase formers, samples with 0, 25 and 50 wt% maltodextrin were sintered at various temperatures. Figure 4 shows the effect of fugitive on LSM, and LSM+V₂O₅. These graphs show that sintering a 50 wt% maltodextrin specimen at ~1300°C results in samples with ~50% density, under conditions that assure that the solid LSM webs are 90-100% dense, which should assure that the pores within the webs are closed to the gas streams. As tape cast specimens of these compositions become available, samples will be provided to UMR for characterization (e.g., mercury porosimetry, SEM, etc.) and YSZ film deposition studies.



INTERFACIAL LAYER DEVELOPMENT

The above work provides a solid foundation for NexTech's interfacial layer development under the UMR subcontract. Parallel to NexTech's development of tape cast LSM substrates that meet the bulk porosity requirements for gas transport, NexTech will focus effort on providing a smooth top surface for subsequent deposition of YSZ films at UMR. Specifically, NexTech will adapt its colloidal process to deposit thin and LSM/SDC coatings onto the top surface of the porous LSM substrates, either prior to or after sintering. From previous work in developing thin film deposition methods, it has been shown that nanoscale aqueous suspensions obtained via hydrothermal processing provide excellent sinterability and a direct processing route to dense, highly uniform, films. By adjusting the composition and particle size distribution of the spray solution, it should be relatively straightforward to adapt the existing processes to produce highly porous composite films with good mixing of LSM and SDC. As a first step, colloidal suspensions of SDC have been produced. A particle size distribution is shown in Figure 5.

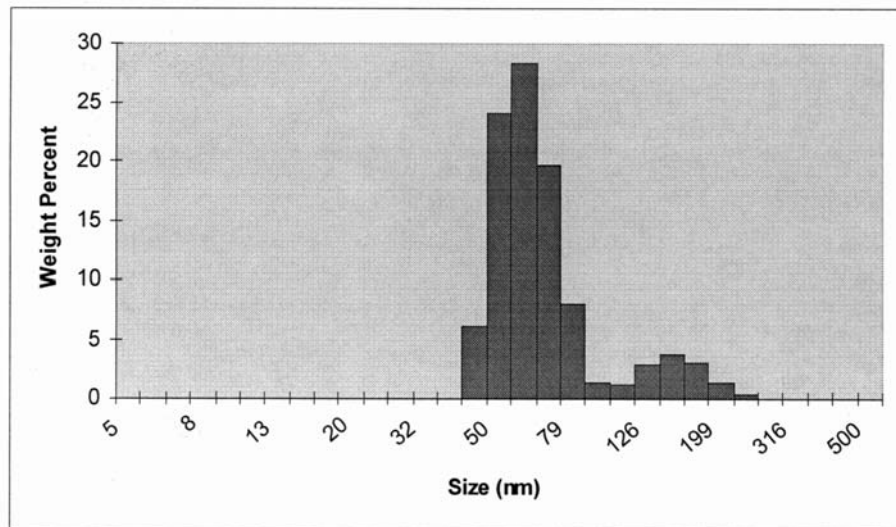


Figure 5. Particle Size Distribution of SDC Material for Colloidal Deposition

In future work, LSM material will be added to these suspensions, and their suitability for depositing the interfacial layer evaluated.

CONCLUSIONS

Significant progress has been made in identifying the compositional systems for the bilayer substrate components. New means of improving the porosity distribution in the substrates have been developed and current work is directed toward developing complementary coating suspensions and substrates.

Task 2.3: Basic Electrical Characterization and Testing of Planar Single Cells

2.3.1: Brief Review of Impedance Spectroscopy

(Zack Byars)



Outline

- Introduce Impedance Spectroscopy
- Explain Fuel cell losses at the cathode
- Techniques to measure these losses.
 - § I vs. V
 - § Impedance Spectroscopy
 - § Combination
- Questions?

1



What is Impedance Spectroscopy?

- AC Conductivity
 - Š If a variable voltage (ac) is applied to a material the impedance is defined as:

$$Z = \frac{V}{I}$$

- A material's impedance changes as the frequency of the applied voltage changes.
 - Š These changes are due to the physical structure of the material and the chemical processes in it.
- Impedance Spectroscopy is where the impedance of a material is measured and the results are related to its chemical and physical properties.

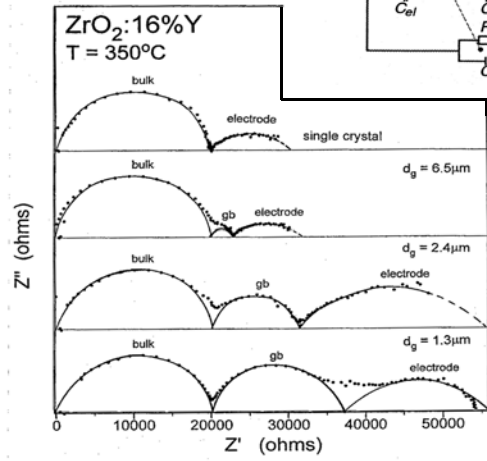
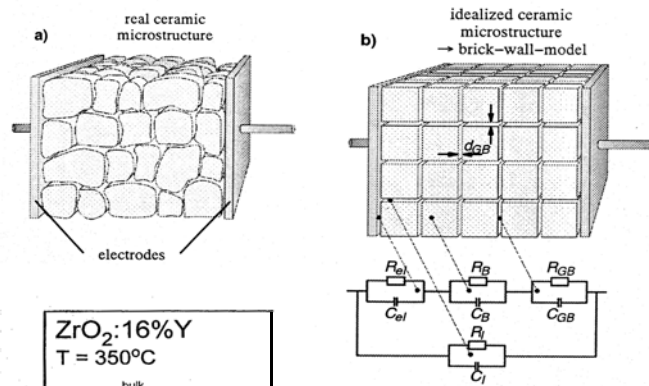


Applications to Impedance Spectroscopy

- Estimating the strength of cement
- Measuring the amount of corrosion of paint.
- Measuring the integrity of organs during transplant.
- Measuring the grain boundary thickness.
- Identifying the chemical processes which take place in batteries.



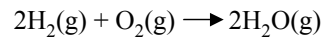
Brick Model- YSZ





Basic Principles of SOFCs

- SOFC are based on the reaction:



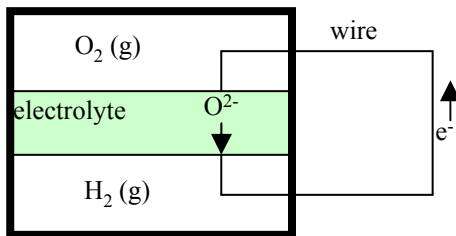
- If H_2 and O_2 gas are mixed together heat is released but electricity is not generated.

- Generation of Electricity

- § Separate the gases with a material which conducts ions, but not electrons, (electrolyte).

- § Connect each side of the electrolyte with a wire.

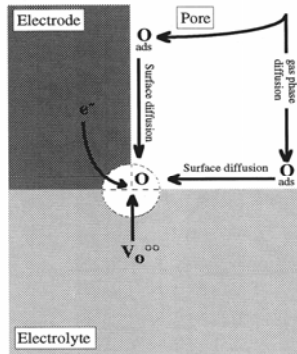
- § The energy of the reaction will force electrons to travel through the wire.





Cathode Reactions

- For current to flow through a fuel cell the following reactions must take place at the cathode:



Oxygen gas diffusion to the surface.

Oxygen absorption onto the surface.

Oxygen surface diffusion.

Dissociation of oxygen molecules to oxygen atoms.

Diffusion of electrons in the cathode.

Bulk oxygen diffusion.

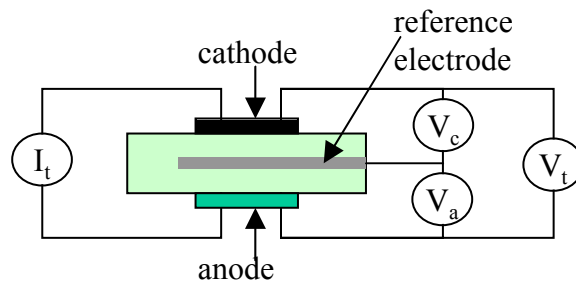
Charge transfer reaction.

- These reactions result in losses which are called overpotentials



Standard Fuel Cell Test Setup

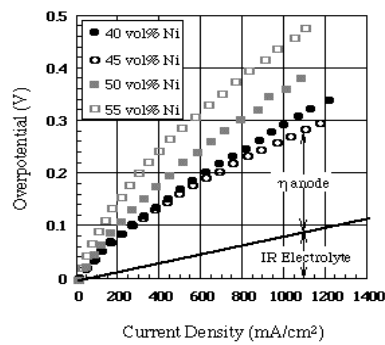
- 5 point conductivity measurements
- Current is measured using one set of leads.
- Voltage is measured using another.
- The reference electrode is inside the electrolyte.
 - Š The reference electrode is used to separate the anode and cathode losses.





Standard Results

- The load resistance is changed to vary the current through the cell.
- Cathode and anode overpotentials can be measured as a function of current.
- Different types of overpotentials can't be separated.



Initial η -j relations of Ni-YSZ cermets sintered at 1400°C.



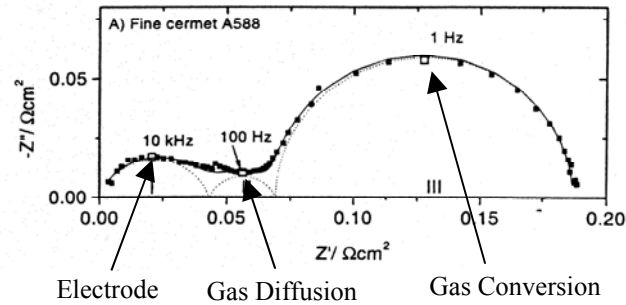
Standard Impedance Spectroscopy of Fuel Cells

□ Procedure

Š A 20mV AC voltage is passed through a fuel cell.

Š No current (on average) is allowed to pass through the cell.

Š If the rate constants for the reactions are different overpotentials can be separated.



9

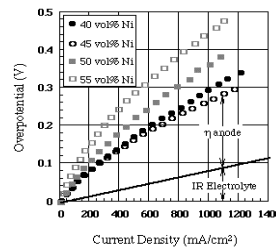


Problems with Standard Impedance Spectroscopy

- Wide range of results
 - § Some papers report as little as 1 arc for anodes, or as many as 5.

- This method assumes overpotentials are not a function of current. THIS IS COMPLETELY NOT TRUE.
 - § Overpotentials follow the Tafel eq.

$$\eta = \frac{RT}{2F} \ln\left(\frac{j}{j_0}\right)$$



Initial η - j relations of Ni-YSZ cermets sintered at 1400°C.

10

2.3.2: Specimen Preparation for Electrode and Single Cell Characterization

(Zack Byars)

INTRODUCTION

Solid oxide fuel cells (SOFC) offer several advantages over current electrical power generation technology. They are more efficient, give off less pollution, and have the potential to be more reliable and less expensive. Currently fuel cells operate at 1000°C. Decreasing the temperature to 800°C or below should allow metals to be used to for the interconnect, thereby reducing cost, increasing durability, and extending service life.

Several things must be done to reduce the operating temperature. The electrodes must be optimized for the lower temperatures, in particular, their catalytic activity must be increased. Also, the electrolyte's conductivity must be increased, or its thickness must be reduced. In this investigation a 30 μ m self-supported yttrium stabilized zirconia (YSZ) electrolyte with La_{1-x}Sr_xCo_{1-y}Fe_yO₃, (LSCF) and La_{1-x}Sr_xMnO₃ (LSM) cathodes and Ni YSZ, Ni-CeO₂, Cu-YSZ, Cu-CeO₂, Ag-YSZ, and Ag-CeO₂ anodes were investigated.

EXPERIMENTAL PROCEDURE

Electrolyte

Tape casting was used to create a 30 μm thick, self-supporting, electrolyte. The electrodes were applied by screen printed onto the dense electrolyte. Commercially available 8 mole percent YSZ (Zirconia Sales of America), with a primary particle size of 0.25 μm and a BET surface area of 8.0 m^2/g , was used to fabricate the electrolyte. The YSZ powder was dried at 150 $^\circ\text{C}$ for at least 24 hours to remove any absorbed water. It was then mixed with a tapecast binder and solvent system from Ferro Corp, B73210, and ball milled for 24 hours. The slurry was then slow rolled for at least 24 hours to remove any trapped air. Next, the slurry was tapecast onto a glass surface with a doctor blade height of 130 μm and a casting speed of 1 cm/s . After the tape dried, a platinum reference electrode was screen printed on the tape while it was still on the glass. Another layer of YSZ was then cast at the same speed on top of the first with a doctor blade height of 140 μm . The tape was then removed from the glass and punched out into 4.44 cm circles. Next, it was sintered at 1450 $^\circ\text{C}$ for one hour with $\approx 0.16\text{g}/\text{cm}^2$ weight on top of it to prevent warping. The tape is typically 30 μm thick after firing.

Cathode

LSCF powder was synthesized by the glycine nitrate technique. Thermogravimetrically $\text{La}_2(\text{CO}_3)_3$, SrCO_3 , $\text{Fe}(\text{NO}_3)_3$, and $\text{Co}(\text{NO}_3)_2$ (Alfa Aesar) were dissolved in water and nitric acid. The amino acid glycine is added to the solution to complex with the metal ions to prevent precipitation, and act as a fuel during charring. When the solution is heated about to 180 $^\circ\text{C}$ the glycine will auto-ignite. Temperatures reach 1100 to 1450 $^\circ\text{C}$ and the mixture is converted into fine, unagglomerated powder. The powders are then mixed with Ferro Corp's BX018-16 resin to make a screen printable paste. The LSCF is screen printed on the electrolyte and fired at temperatures ranging from 800 to 1100 $^\circ\text{C}$ forming the cathode.

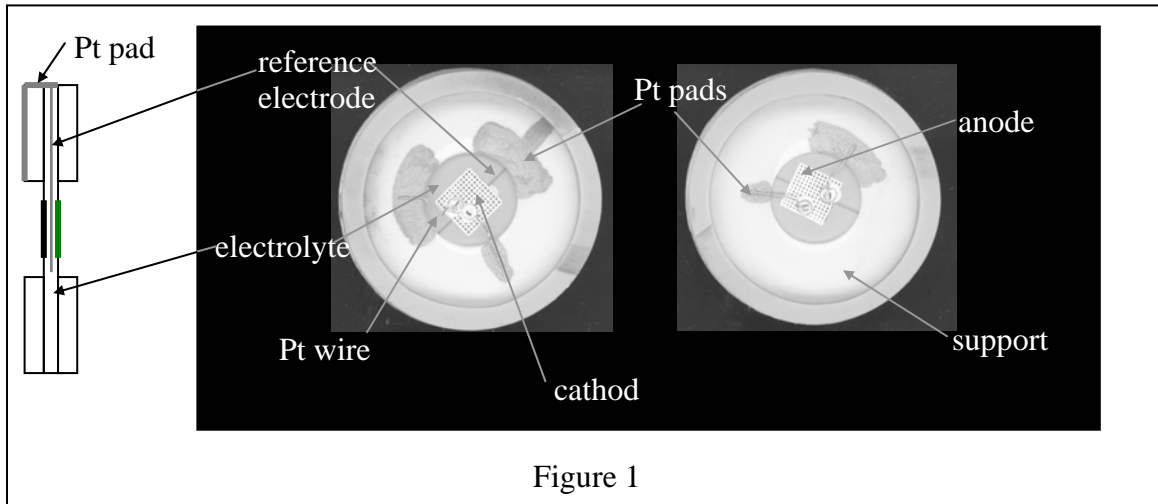
Anode Fabrication

CuO and NiO powders were synthesized by the glycine nitrate technique, as described above, while silver metal was purchased from Alfa Aesar. These powders were then mixed with YSZ with a BET surface area of $\approx 40 \text{ g/cc}$ (Nanomaterials) or Ceria with a BET surface area of $\approx 50 \text{ m}^2/\text{g}$ (Nanophase). Again the powders are mixed with Ferro's resin to make a paste, which is then screen printed on the opposite side of the electrolyte, and fired at temperatures ranging from 700 to 900 $^\circ\text{C}$. The oxide powders will be reduced insitu. Next, platinum or silver current collectors are screen-printed to form a grid pattern on each electrode.

Supports

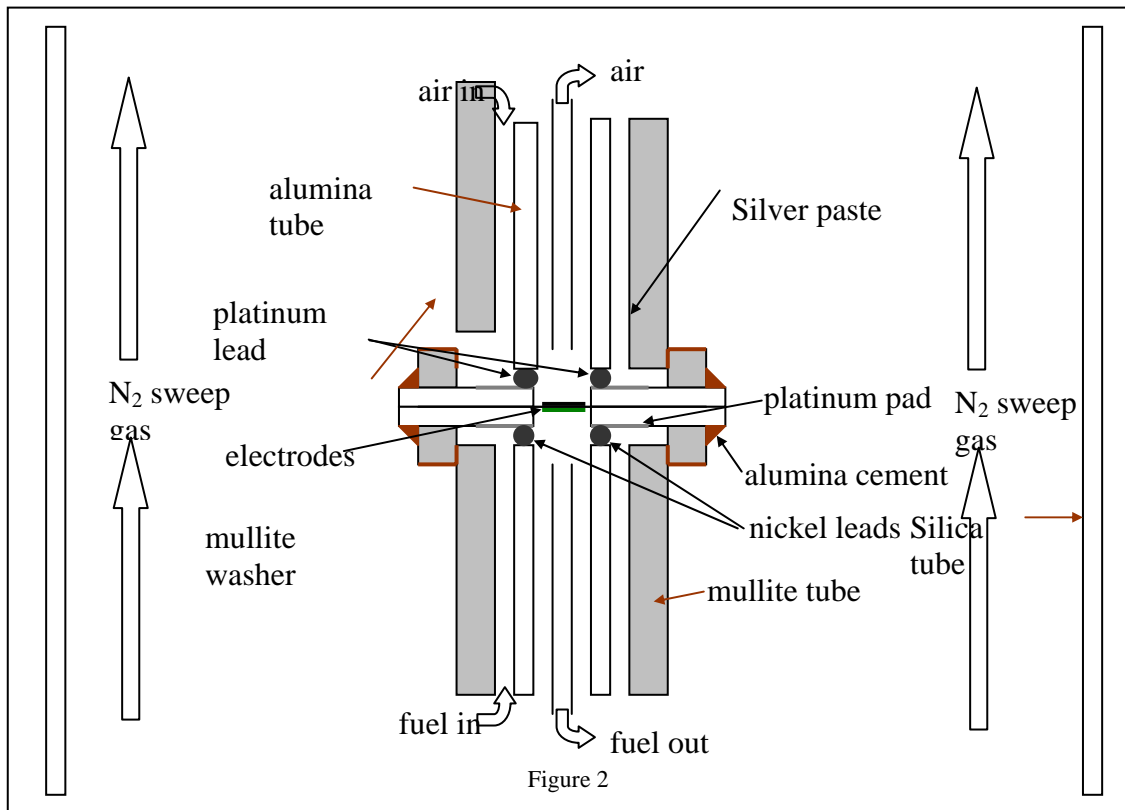
To provide structural integrity 350 μm supports were tape cast and fired at 1450 $^\circ\text{C}$. Platinum pads, which will be used to make electrical connections, were painted on the supports using Platinum paste (Ferro Corp). The paste was then used to bond platinum wires to the pads. The supports were then fired to 1250 $^\circ\text{C}$ to sinter the platinum. The supports and wires were then

connected to the electrolyte using silver paste (Ferro Corp), which was then fired to 700°C, see figure 1.



Sample Mounting and Testing

Mullite rings were superglued to the supports, and then cemented to the mullite tubes using Aremco cement #503, see figure 1 and 2. Platinum wire, inside an alumina thermocouple tube, was used to make electrical contact to the platinum pads on the cathode side. Nickel wire was used on the anode side.



The mullite tubes were then mounted inside a silica tube furnace. The furnace is heated at a rate of 2°C/min to the measurement temperatures (600 to 900°C).

Gas was then fed to the cell. The oxidant and fuel enter the mullite tube opposite the fuel cell. The gas travels down to the cell, and then out through a thermocouple tube. N₂ is used as the sweep gas, to remove any oxidant or fuel leaking out the inner tubes. Gas flow is controlled by four mass flow controllers, and monitored by ball flow meters. Air flowing at 200 sccm was used as the oxidant, and mixture of forming gas (90% N₂, 10% H₂) flowing at 200 sccm and CO₂ flowing at 2.0 sccm was used as the fuel.

RESULTS AND DISCUSSION

A typical cell is shown in figure 3. In this cell the cathode was used as the cathode La_{0.7}Sr_{0.2}MnO₃, and a mixture of NiO and YSZ (40 vol % Ni) was used for the anode. The platinum reference electrode can be seen buried inside the electrolyte, and the current collector is visible on the anode.

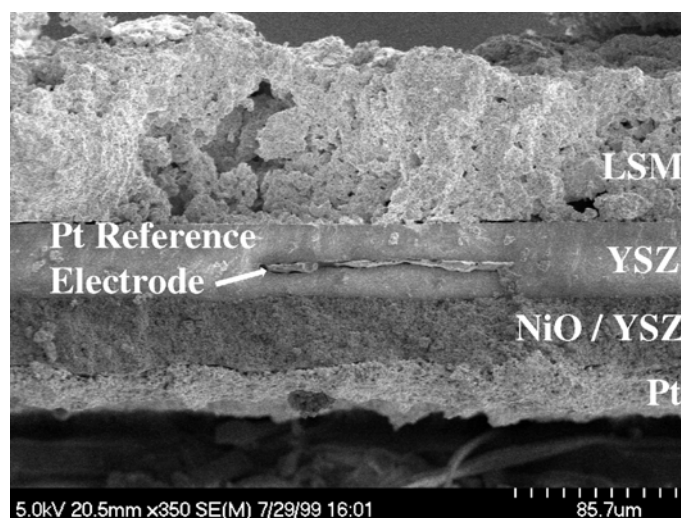


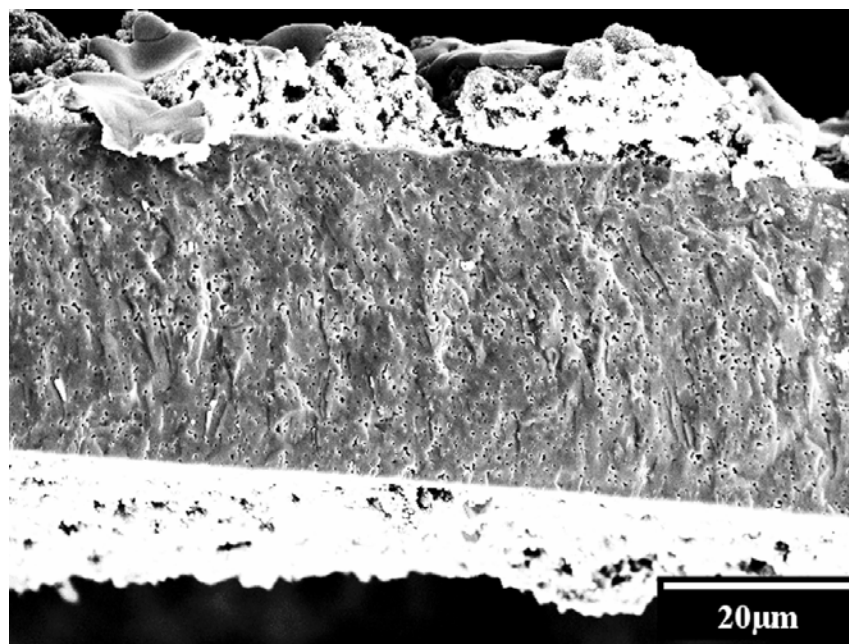
Figure 3 Ref. 2

Plots of power density and electrode overpotential vs. current density will be included in the poster. These results will be compared to impedance spectroscopy of the electrode materials.

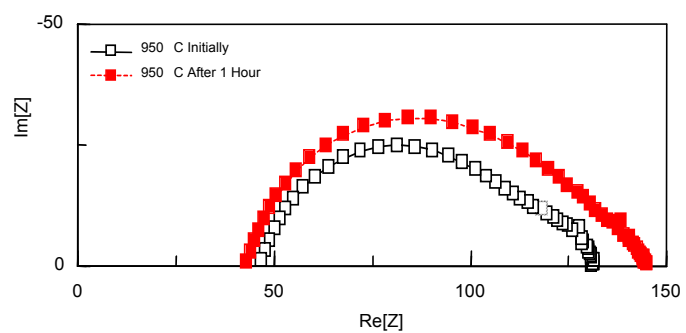
REFERENCES

1. I. Kosacki, B. Gorman and H. U. Anderson, *Electro. Chem. Soc. Proc.* 97-24, 631 (1998)
2. H. U. Anderson, W. Huebner, B.P. Gorman, Z. Byars, and I. Kosacki, *Poster Presentation US DOE* 8/15/1999.
3. H. U. Anderson, L-W. Tai, C. C. Chen, and M. M. Nasrallah, *Ionic and Mixed Conducting Ceramics*, 2nd international symposium, 376 (1994).

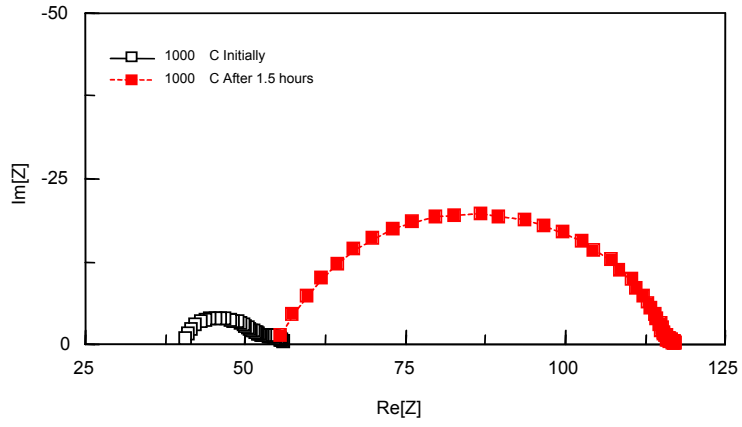
4. H. U. Anderson, L-W. Tai, C. C. Chen, M. M. Nasrallah, and W. Huebner, Solid Oxide Fuel Cells IV, 375 (1995).



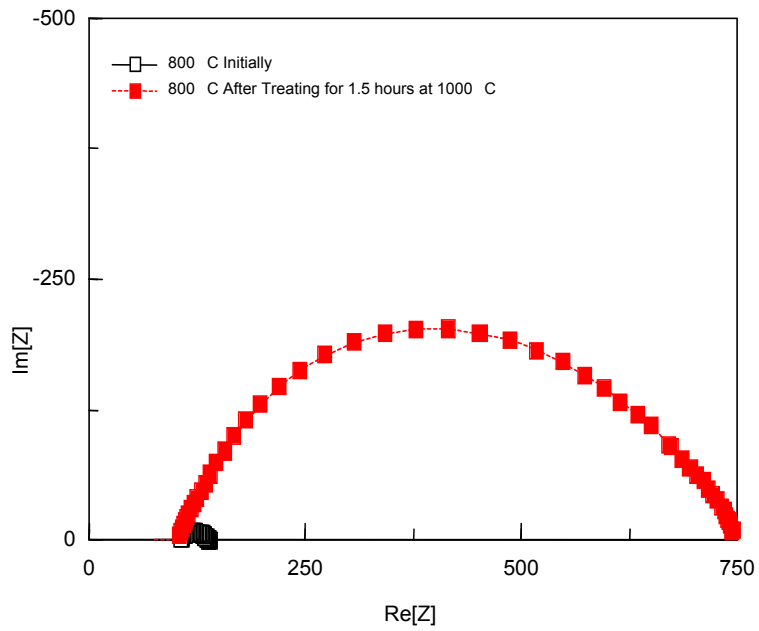
LSCF AND YSZ INTERACTION STUDY
Aging at 950°C



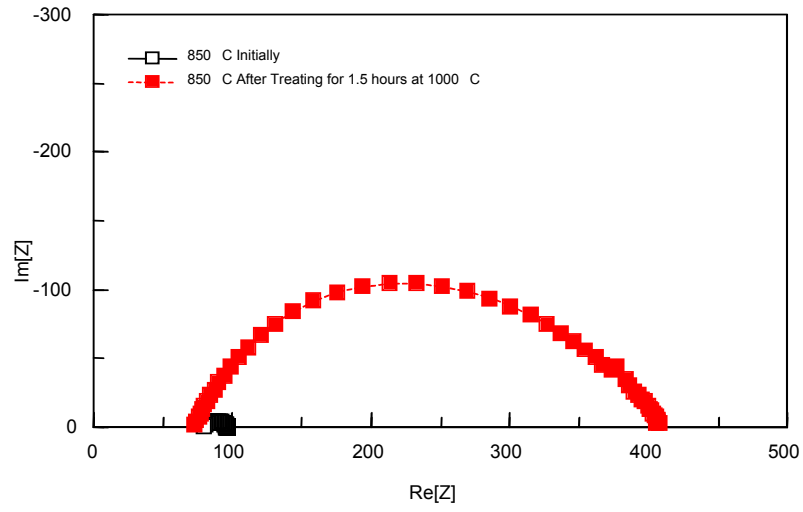
LSCF AND YSZ INTERACTION STUDY
Aging at 1000°C



LSCF AND YSZ INTERACTION STUDY
800°C Before and After Treating at 1000°C



LSCF AND YSZ INTERACTION STUDY
850°C Before and After Treating at 1000°C



LSCF AND YSZ INTERACTION STUDY
900°C Before and After Treating at 1000°C

